Quaternary Science Reviews 243 (2020) 106455

Contents lists available at ScienceDirect

Quaternary Science Reviews

journal homepage: www.elsevier.com/locate/quascirev

Glacial fluctuations in tropical Africa during the last glacial termination and implications for tropical climate following the Last Glacial Maximum

M.S. Jackson [a, *, 1], M.A. Kelly [a], J.M. Russell [b], A.M. Doughty [c], J.A. Howley [d], J.W. Chipman [a], D.A. Cavagnaro [a], M.B. Baber [a], S.R.H. Zimmerman [e], B. Nakileza [f]

[a] Department of Earth Sciences, Fairchild Hall, Dartmouth College, Hanover, NH, 03755, United States
[b] Department of Earth, Environmental, and Planetary Sciences, Brown University, Providence, RI, 02912, United States
[c] Geology Department, Carnegie Hall, Bates College, Lewiston, ME, 04240, United States
[d] New Hampshire Department of Health and Human Services, Concord, NH, 03301, United States
[e] Center for Accelerator Mass Spectrometry, Lawrence Livermore National Laboratory, Livermore, CA, 94550, United States
[f] Mountain Resource Centre, Makerere University, Kampala, Uganda

ARTICLE INFO

Article history:
Received 19 November 2019
Received in revised form
19 June 2020
Accepted 22 June 2020
Available online xxx

Keywords:
Paleoclimatology
Africa
Glacial geomorphology
Cosmogenic isotopes

ABSTRACT

The tropics are a dynamic component of the global climate system and exert a profound influence on modern climate variability. Yet the role of the tropics in past climate changes, for example during the last glacial termination, is uncertain. This uncertainty is due in part to the relative paucity of terrestrial temperature records from the tropics, which hinders efforts to understand the mechanisms that influenced deglacial warming and abrupt climate events. Tropical glaciers are sensitive to changes in climate, and mapping and dating past tropical glacial fluctuations provides a valuable record of terrestrial climate changes in the low latitudes. We report a chronology of past glacial extents in the Rwenzori Mountains of Uganda (0.3°N, 29.9°E) based on 51 beryllium-10 (^{10}Be) surface-exposure ages from three separate glacial catchments. Results indicate that Rwenzori glaciers retreated considerably during Heinrich Stadial 1. The rate of net glacial recession slowed between ~15 and 11 ka, although glaciers continued to retreat during this period. Rwenzori glaciers then retreated more rapidly during the early Holocene. The Rwenzori glacial chronology is broadly similar to glacial chronologies reconstructed elsewhere in East Africa and in tropical South America. We suggest that this similarity may reflect coherent, tropics-wide temperature fluctuations during the last deglaciation. The Rwenzori glacial chronology provides crucial information on the global footprint of deglacial warming and abrupt climate events and, thus, the potential mechanisms that influenced tropical climate during the last glacial termination.

1. Introduction

The termination of the last ice age represents Earth's greatest natural climate warming of the last 100,000 years, yet the mechanisms that initiated and propagated deglacial warming around the globe remain unresolved (Denton et al., 2010). The last glacial termination was punctuated by events such as Heinrich Stadial 1 (HS1; ~18.0–14.6 ka; Barker et al., 2009), the Bølling-Allerød (B-A; ~14.7–12.9 ka; Rasmussen et al., 2006), Antarctic Cold Reversal (ACR; ~14.6–12.8 ka; Lemieux-Dudon et al., 2010), and the Younger Dryas (YD; ~12.9–11.7 ka; Blunier and Brook, 2001), each of which involved reorganizations of oceanic and atmospheric circulation and which featured potentially anti-phased expressions in northern and southern high-latitude proxy records (Rasmussen et al., 2006; Broecker et al., 2010; WAIS Divide Project Members, 2013).

Resolving the global pattern and expression of deglacial warming and abrupt climate events is crucial for understanding the global climate system, its response to past warming, and the mechanisms that cause abrupt climate change. However the spatial distribution of deglacial temperature records is not uniform, and there is a paucity of terrestrial paleotemperature records from the

---

* Corresponding author.
E-mail address: margaret.jackson@nuigalway.ie (M.S. Jackson).

[1] Current Affiliation: School of Geography, Archaeology, and Irish Studies, National University of Ireland, Galway, University Road, Galway, H91 TK33, Ireland.

https://doi.org/10.1016/j.quascirev.2020.106455
0277-3791/

tropics (23°N-23°S). The tropics comprise nearly half of Earth's surface and are the primary source of latent heat and water vapor to the global atmosphere (Pierrehumbert, 2000). Through phenomena such as the El Niño Southern Oscillation (ENSO) the tropics are also a dominant control on modern climate variability (e.g., Sobel and Bretherton, 2000; Diaz et al., 2003). The tropics are thus a key, dynamic element of the global climate system. Understanding their role in deglacial warming and abrupt climate events is crucial for understanding global climate changes.

Glacial mass balance in the humid inner tropics (~10°N-10°S) is controlled primarily by temperature (Kaser and Osmaston, 2002; Taylor et al., 2006; Rupper and Roe, 2008; Sagredo et al., 2014; Doughty et al., in press). Past tropical glacial extents therefore provide a valuable proxy for terrestrial paleotemperature change (Jomelli et al., 2014). Recent applications of cosmogenic nuclide surface-exposure dating of glacial deposits in tropical South America suggest that glaciers there retreated during part of HS1 (e.g., Bromley et al., 2016; Mark et al., 2017) and were more extensive during the B-A/ACR than the YD (Jomelli et al., 2014, 2017; Mark et al., 2017; Stansell et al., 2017). The lack of similar glacial extent records from elsewhere in the low latitudes, however, leaves the spatial variability of deglacial climate change unclear.

To address the wider pan-tropical signal of glacial fluctuations during the last glacial termination, we report a new chronology of past glacial extents in the equatorial Rwenzori Mountains in Uganda (Fig. 1). The chronology comprises 51 beryllium-10 (^{10}Be) surface-exposure ages, from glacial deposits in three separate valleys, which span the last deglaciation. These data illuminate the timing and magnitude of glacial fluctuations in the Rwenzori. We then compare our results from the Rwenzori with records of glacial fluctuations elsewhere in East Africa and with similar ^{10}Be surface-exposure glacial chronologies from tropical South America to assess the potential coherence of glacial and terrestrial climate changes across the tropics during the last glacial termination.

2. Background

2.1. Geologic setting and previous work

The Rwenzori Mountains (0.3°N, 29.9°E) are an uplifted horst of crystalline basement on the border between Uganda and the Democratic Republic of Congo (Fig. 1). The highest peak in the Rwenzori, Mt. Stanley, is 5109 m asl and stands roughly 360 m above the modern freezing level of ~4750 m asl (Lentini et al., 2011). The slopes of the Rwenzori receive up to ~2.0–2.7 m precipitation each year, with two distinct wet seasons during the boreal spring and autumn as the Intertropical Convergence Zone (ITCZ) passes overhead (Osmaston, 1989; Singarayer and Burrough, 2015). Evergreen afro-alpine and montane vegetation dominate in the Rwenzori, with a marked altitudinal zonation in vegetation regimes (Foster, 2001; Osmaston, 2006). Bare bedrock exposure is limited mostly to areas above 4000 m asl.

Evidence of past glacial fluctuations in the Rwenzori comes in the form of a variety of glacial deposits, including abundant and widespread moraines. Osmaston (1965, 1989) conducted extensive glacial-geomorphic mapping in the Rwenzori and, from this work, classified glacial moraines into five distinct stages based on their inferred relative ages. These stages, from the oldest to youngest, include the Katabura, Rwimi, Lake Mahoma, Omurubaho, and Lac Gris. In this paper we focus on the Lake Mahoma and Omurubaho stage moraines. The Lake Mahoma stage moraines are high-relief (30–100 m high) ridges, including many well-preserved lateral moraines, that extend as low as ~2000 m asl. Osmaston (1989) estimated the Lake Mahoma stage moraines to be at least ~15 ka

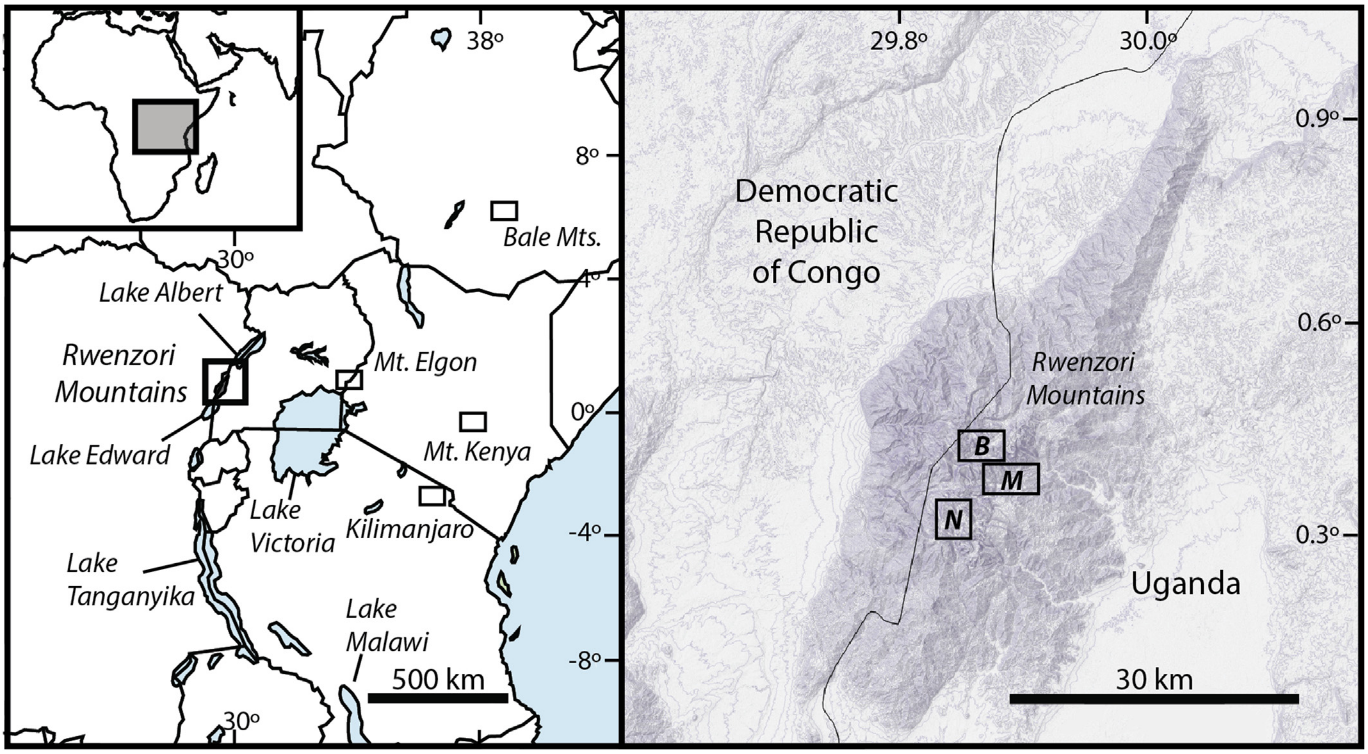

Fig. 1. Map of East Africa and locations mentioned in the text (left). The Rwenzori Mountains are located on the border between Uganda and the Democratic Republic of Congo (black box marks location of the Rwenzori and denotes bounds of right-hand panel). Other glacierized or formerly glaciated sites in the region include Uganda's Mt. Elgon, Kilimanjaro in Tanzania, Mt. Kenya in central Kenya, and the Bale Mountains on the Ethiopian plateau. We targeted glacial deposits in three Rwenzori catchments (right): the Mubuku (M), Bujuku (B), and Nyamugasani (N) valleys. Boxed areas correspond to field areas detailed in Figs. 4–6.

in age. The Omurubaho stage moraines are lower relief (3–30 m high), occur at elevations ~3600–4000 m asl, and are stratigraphically inboard of Lake Mahoma stage moraines. Although Osmaston (1989) estimated that these moraines formed during the Holocene, he refrained from placing more precise age constraints on the deposits.

Until recently, the only numerical age control on Rwenzori glacial fluctuations during the last termination came from two radiocarbon ages of high-alpine lake sediments. Lake Mahoma (~3000 m asl), located in the lower Mubuku valley, is dammed by Lake Mahoma stage moraines. Livingstone (1962) reported a radiocarbon age of ~17.5 cal kyr BP (14,750 ± 290 ^{14}C yr) from the bottom 20 cm of organic-rich sediments which overlie inorganic silts in Lake Mahoma. This date provides a minimum-limiting age on deglaciation from the Lake Mahoma stage moraines. Upper Lake Kitandara (~4000 m asl), located in the Butahu valley, is not associated directly with moraines and may have been formed as a result of rockfall damming the lake basin. Livingstone (1967) reported a radiocarbon age of ~7.7 cal kyr BP (6890 ± 100 ^{14}C yr) from bulk organic matter in the basal sediments in Upper Lake Kitandara. This date provides a minimum-limiting age of deglaciation of the site.

Recent applications of ^{10}Be surface-exposure dating (hereinafter ^{10}Be dating) in the Rwenzori provide direct constraints on the timing of past glacial fluctuations during the Last Glacial Maximum (LGM; ~26.5–19 ka). Eight ^{10}Be ages of boulders on two Lake Mahoma stage moraines in the lower Mubuku valley near Lake Mahoma indicate deposition at ~21.5 and ~24.9 ka, during the global LGM (Kelly et al., 2014). More detailed mapping and dating of these moraines indicates expanded glaciers from ~29.0 ka to 21.5 ka in Mubuku valley and until ~18.9 ka in the more southern Moulyambouli valley (Jackson et al., 2019). The timing and extent of glacial fluctuations in the Rwenzori following the LGM, however, remain unresolved (Kaser and Osmaston, 2002).

2.2. Study sites

We focused our work in three Rwenzori catchments, each of which contain glacial deposits amenable for ^{10}Be dating. These are the Mubuku, Bujuku, and Nyamugasani valleys, described in more detail below.

2.2.1. Bujuku valley

The Bujuku valley trends eastward from the area between Mt. Baker, Mt. Stanley, and Mt. Speke before turning southeast toward the Mubuku-Bujuku Rivers' confluence (Figs. 1 and 2). The southern side of the valley floor is composed primarily of volcanic lithologies whereas the northern side of the valley, including the slopes of Mt. Speke, are predominantly gneissic (McConnell, 1959). The valley walls are steep and, in the upper valley near Lake Bujuku, they are obscured by scree and rockfall deposits (Fig. 2). Where unobscured by vegetation, glacial molding and striations are visible on the bedrock valley walls and floor. Above the Mubuku-Bujuku Rivers' confluence are a series of Lake Mahoma stage moraines deposited on steep valley walls (Osmaston, 1989). Eight kilometers upvalley from the Mubuku-Bujuku Rivers' confluence a large (~1 km wide) wetland, the Bigo Bog, marks an infilled reach of the valley at the confluence of multiple catchments (Osmaston, 1989)(Fig. 2). The bog is bounded on both its up- and downvalley sides by Omurubaho stage moraines (Osmaston, 1989). Additional Omurubaho stage moraines occur ~1.5 km upvalley of Bigo Bog. No other moraines are preserved between these Omurubaho deposits and presumed historical-age deposits on the slopes of Mt. Speke and Mt. Baker (Osmaston, 1989).

2.2.2. Mubuku valley

The eastern flank of Mt. Baker (4844 m asl) marks the head of the Mubuku valley (Figs. 1 and 2). The valley trends east-west and its upper reaches are bounded by steep, faulted bedrock walls composed of strongly foliated gneisses (McConnell, 1959). The lower Mubuku valley is marked by large (>100 m high) Lake Mahoma stage lateral moraines (Osmaston, 1989) dated to ~29.0–21.5 ka (Kelly et al., 2014; Jackson et al., 2019) that formed where ice from the Mubuku and Bujuku valleys coalesced during the LGM. Deglaciation from the LGM maximum extent began ~21.5 ka (Kelly et al., 2014; Jackson et al., 2019). Inboard of these LGM deposits, additional lower-relief (10–30 m high) moraines occur along the valley floor up to ~3000 m asl. Many of these moraines are bisected by the Mubuku River and all are classified as Lake Mahoma stage deposits by Osmaston (1989). These include one right-lateral moraine in the central Mubuku valley ~1.5 km inboard of the Mubuku-Bujuku Rivers' confluence that dates to ~17.9 ka (Jackson et al., 2019). No Omurubaho-stage moraines occur upvalley of the Lake Mahoma stage moraines.

2.2.3. Nyamugasani valley

The southward trending Nyamugasani valley extends from Mt. Weisman (4619 m asl) to the southern edge of the Rwenzori massif, where prominent Lake Mahoma stage moraines rise at least 100 m above the Nyamugasani River (Fig. 1). The valley is underlain by migmatic gneiss and granite with some areas of amphibolite (McConnell et al., 1959). The upper reach of the Nyamugasani valley contains numerous lakes, some of which are dammed by bedrock and some by Omurubaho stage moraines (Fig. 2). The upper Nyamugasani valley walls are less steep than those in the Mubuku and Bujuku valleys. Exposed, glacially molded bedrock is readily visible along areas of the valleys walls and floor, although much of the valley floor is infilled with lakes and wetlands.

3. Methodology

Fieldwork took place over four field seasons between 2009 and 2016, during which we identified and classified glacial-geomorphic features based on their morphology, weathering characteristics, and relative (stratigraphic) position (Tables 1 and 2). We also utilized 0.5-m resolution WorldView-1 satellite imagery to aid in identifying and contextualizing glacial features and then constructed detailed glacial-geomorphic maps of the field area with these data. All glacial-geomorphic maps are drawn onto a 30-m resolution digital elevation model of the Rwenzori massif.

We collected samples for ^{10}Be dating from the uppermost surfaces ($\leq$5 cm) of boulders on moraines and boulders set down on bedrock using a hammer and chisel or the "drill-and-blast" method of Kelly (2003). We selected boulders that showed no indication of post-depositional movement or alteration and recorded their locations using a handheld GPS (±3 m vertical, ± 1 m horizontal; Table 2). We prioritized sampling flat rock surfaces with no surface dip in order to minimize potential uncertainties in the shielding correction. Where necessary, we measured the rock-surface dip and dip direction using a handheld compass. We recorded topographic shielding using a handheld clinometer (Table 2). Where low clouds prevented the measurement of topographic shielding in the field, we estimated shielding values using a 30-m digital elevation model of the Rwenzori. This method yielded shielding values similar (within ~2%) to those based on field measurements.

We crushed the rock samples and used a series of H_3O_4P/NaOH and HF/HNO_3 leaches to purify quartz from the crushed 250–710 μm size fraction. We spiked the samples and process blanks with a known amount of beryllium-9 (Table 3) and used a modified version of the methods described in Schaefer et al. (2009)

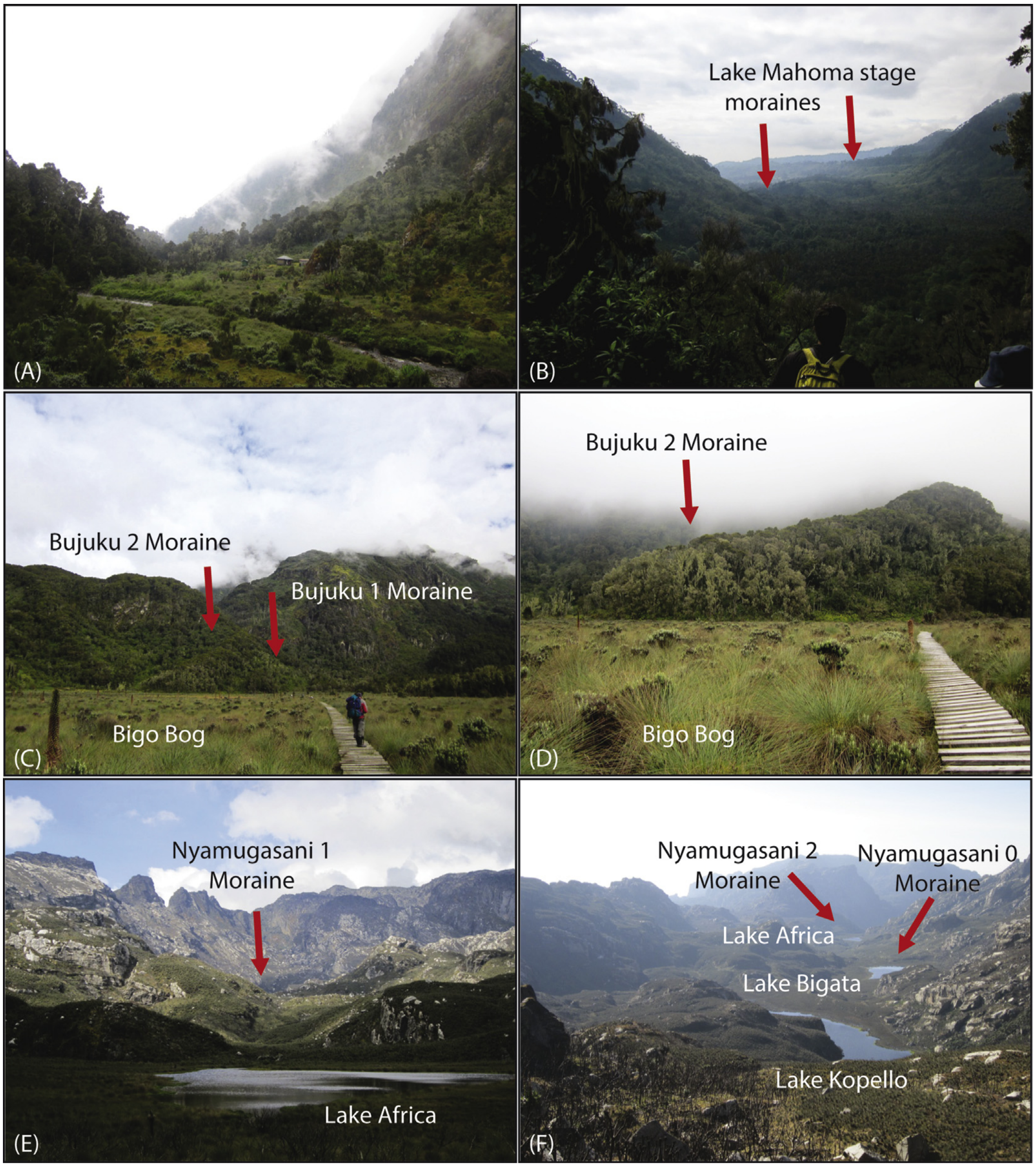

Fig. 2. (A) The Guy Yeomen hut is in the upper reach of the Mubuku valley, which is bounded by steep, faulted bedrock walls. (B) The Mubuku valley floor contains numerous moraine forms, though it is primarily infilled by wetland. View is toward the southeast. (C) In the Bujuku valley, Bigo Bog marks the confluence of multiple catchments and is bounded by steep, gneissic bedrock walls. Moraines border much of the bog perimeter. View is toward the west. (D) Many moraines in and surrounding Bigo Bog, including the Bujuku 2 moraine, plunge into the modern bog surface. View is toward the west. (E) In the upper Nyamugasani valley, Lake Africa (foreground) is one of two moraine-dammed lakes. The peak of Mt. Weisman (distance) marks the head of the valley. View is to the north. (F). The Nyamugasani valley, with view to the south. Lake Kopello, dammed by bedrock, is visible in the foreground, with the moraine-dammed Lakes Bigata and Africa in the distance. Moraines are highlighted by red arrows.

to isolate beryllium from the samples and process blanks (Tables 2 and 3). All sample preparation took place at the Dartmouth College Cosmogenic Nuclide Laboratory. Beryllium ratios were measured at the Lawrence Livermore National Laboratory Center for Accelerator Mass Spectrometry and normalized to the 07KNST3110 standard (Nishiizumi et al., 2007).

We calculated the Rwenzori ^{10}Be ages using a high-elevation, low-latitude production rate (Kelly et al., 2015) and time-invariant (“St”) scaling (Lal, 1991; Stone, 2000) using version 3 of the online exposure-age calculator described by Balco et al. (2008 and subsequently updated). Two ^{10}Be production rate calibration datasets from high-elevation, low-latitude sites (Blard et al., 2013; Kelly et al., 2015) yield the most accurate and precise results (lowest uncertainty by total scatter; Balco et al., 2008) when paired with “St” scaling; all ^{10}Be ages included within the results and discussion text are ages as calculated using “St” scaling and are presented in years before present (yr BP) relative to the year of sample collection (Tables 1 and 2). We also report ^{10}Be ages calculated using an alternative, time-dependent scaling framework (“LSDn” scaling; Lifton et al., 2014) in Table 1. There is a maximum ~4.5% difference in the ^{10}Be ages calculated with these two methodologies, although we note that the choice of scaling framework used does not alter our overall interpretations. New ^{10}Be production rate calibrations, if and when available, may alter the ^{10}Be ages and interpretations presented here.

We measured certain samples multiple times (that is, we isolated and measured beryllium in two separate quartz aliquots from the same rock sample) in order to check for consistency in

Table 1
Surface-exposure ages. Samples are listed according to valley, landform, sample name, and corresponding map identification number (as in Figs. 4–6). ^{10}Be ages are calculated using the high-altitude, low-latitude production rate of Kelly et al. (2015) and are presented using both time-invariant “St” scaling (Lal, 1991; Stone, 2000) and time-variant “LSDn” scaling (Lifton et al., 2014). Sample ages considered to be outliers are presented in italics. Arithmetic-mean moraine ages are calculated using time-invariant “St” ages and include only primary sample measurements. All ^{10}Be ages are presented with both one-sigma ‘internal’ uncertainty (int; ^{10}Be measurement uncertainty), and ‘external’ or total uncertainty (ext; uncertainty inclusive of all age calculation parameters).

Map ID	Landform	Sample ID	Age (St)	± (int; St)	± (ext; St)	Age (LSDn)	± (int; LSDn)	± (ext; LSDn)	Mean (St)	Std. Dev.	Std. Err.
Mubuku valley											
1	Mubuku 0	RZ-16-41	11,170	280	690	11,290	280	710			
2	Mubuku 0	RZ-16-43	13,790	350	850	13,670	340	860			
3	Mubuku 0	RZ-16-44	12,600	330	780	12,680	330	800	12,520	1,310	760
Bujuku valley											
4	*Bujuku 8*	*RZ-16-07*	*2,190*	*290*	*310*	*2,650*	*350*	*380*			
5	*Bujuku 8*	*RZ-16-08*	*13,860*	*400*	*880*	*13,890*	*410*	*900*			
6	Bujuku 7	RZ-16-02	16,770	310	1000	16,330	310	990			
7	Bujuku 7	RZ-16-03	15,370	370	950	15,110	370	950			
8	*Bigo Drift*	*RZ-16-09*	*11,200*	*350*	*720*	*11,190*	*350*	*740*			
9	Bigo Drift	RZ-16-11	16,130	480	1,030	15,450	460	1,010			
10	*Bigo Drift*	*RZ-16-13*	*22,750*	*460*	*1,370*	*20,770*	*420*	*1,270*			
11	*Bujuku 6*	*RZ-16-24*	*9,490*	*270*	*600*	*9,770*	*270*	*630*			
12	*Bujuku 6*	*RZ-16-25*	*13,800*	*360*	*860*	*13,430*	*350*	*850*			
13	Bujuku 5	RZ-16-21	15,490	340	940	14,850	320	920			
14	Bujuku 5	RZ-16-26	14,930	320	900	14,390	300	890	15,210	390	280
15	Bujuku 4	RZ-16-17	15,380	410	960	14,810	390	940			
16	Bujuku 4	RZ-16-18	14,860	400	930	14,340	390	920	15,120	370	260
17	Bujuku 3	RZ-16-14	14,090	420	900	13,740	410	890			
18	Bujuku 2	RZ-12-11	15,540	300	930	14,870	280	910			
19	Bujuku 2	RZ-12-12	14,700	280	880	14,150	270	860			
20	Bujuku 2	RZ-12-13	13,920	260	830	13,550	260	830			
	Bujuku 2	RZ-12–13x	13,550	260	810	13,200	250	800	14,720	810	470
21	Bujuku 1	RZ-12-14	14,010	300	840	13,630	290	840			
22	Bujuku 1	RZ-12-15	14,060	230	830	13,670	220	820			
23	Bujuku 1	RZ-12-16	14,310	280	860	13,870	270	850	14,130	160	90
24	Bujuku 0	RZ-12-17	11,500	220	690	11,280	210	690			
25	Bujuku 0	RZ-12-18	12,180	380	780	11,840	370	780			
26	Bujuku 0	RZ-16-31	11,550	230	690	11,310	220	690	11,740	380	220
27	*Bujuku Slide*	*RZ-16-35*	*12,360*	*230*	*730*	*11,920*	*220*	*720*			
28	Bujuku Slide	RZ-16-36	11,030	210	660	10,930	200	660			
29	Bujuku Slide	RZ-16-39	11,030	210	660	10,930	200	660			
Nyamugasani valley											
30	Katunda boulder	RZ-15-05	14,110	270	840	13,530	260	830			
31	Katunda boulder	RZ-15-06	13,780	230	810	13,220	220	800			
32	Nyamugasani 2	LA-2	11,560	220	690	11,270	220	690			
33	Nyamugasani 2	LA-1	12,730	280	770	12,310	270	760			
	Nyamugasani 2	LA-1x	12,250	370	790	11,820	360	770			
34	Nyamugasani 2	LA-3	12,490	240	750	12,060	230	740			
35	Nyamugasani 2	LA-5	11,780	220	700	11,390	220	690			
	Nyamugasani 2	LA-5x	11,620	190	680	11,280	190	680	12,140	560	280
36	Nyamugasani 1	RZ-12-33	11,520	220	690	11,210	210	680			
37	Nyamugasani 1	RZ-12-34	11,380	210	680	11,130	210	680			
38	Nyamugasani 1	RZ-12-36	11,270	210	670	11,060	210	670			
39	Nyamugasani 1	RZ-12-37	11,150	230	670	10,990	230	680	11,330	160	80
40	Nyamugasani 0	RZ-12-38	11,660	220	690	11,300	210	690			
41	Nyamugasani 0	RZ-12-39	11,040	210	660	10,910	210	660			
42	Nyamugasani 0	RZ-12-41	11,140	210	660	10,980	210	670			
43	Nyamugasani 0	RZ-12-44	11,020	280	680	10,890	270	690	11,220	300	150
44	Kopello boulder	KOP-1	10,450	270	650	10,390	270	660			

(*continued on next page*)

Table 1 *(continued)*

Map ID	Landform	Sample ID	Age (St)	± (int; St)	± (ext; St)	Age (LSDn)	± (int; LSDn)	± (ext; LSDn)	Mean (St)	Std. Dev.	Std. Err.
45	Kopello boulder	KOP-2	11,770	290	720	11,360	280	710			
46	Kopello boulder	KOP-4A	12,080	340	760	11,600	320	740			
47	*Kopello boulder*	*KOP-5*	*8,300*	*210*	*510*	*8,220*	*200*	*520*			
48	Kopello boulder	RZ-15-12	11,030	210	660	10,900	210	660			

beryllium ratios. The secondary sample measurements (aliquot ‘x’) are reported in Tables 1 and 3. We do not include these data in our analysis or discussion, and these samples are not assigned Map ID numbers in Tables 1–3

For each landform with multiple ^{10}Be ages, we report arithmetic-mean moraine ages with the associated standard error of the mean and standard deviation in Table 1. We interpret the mean moraine ages as the time of ice recession following a glacial readvance or stillstand (i.e., the cessation of sediment deposition on the moraine). Where ^{10}Be ages of landforms are out of stratigraphic order with other dated deposits up or downvalley, or samples do not yield a single age population, we report individual ^{10}Be ages rather than a mean moraine age. We do not report mean ages for populations of boulders on bedrock, which we interpret as the time of ice thinning or retreat past a given position rather than the age of a discrete landform.

We did not correct the ^{10}Be ages for the potential influence of boulder surface erosion or cover by snow. Many boulders featured granular surface textures and, in some cases, showed evidence of exfoliation. The apparent degree of weathering, however, was variable among individual boulders and among lithologies. Prior work using ^{10}Be dating in the Rwenzori showed that raised quartz veins and boulder surfaces on the same moraine yield statistically similar ages (for LGM-age deposits; Jackson et al., 2019). Due to the uncertainty in erosion rates and the apparently negligible influence of erosion on ^{10}Be ages of LGM moraines, we refrain from correcting the ^{10}Be ages reported here for erosion. We note that snow likely does not persist for a considerable length of time at the sample sites due to the intense equatorial solar radiation and warm daytime temperatures.

We also did not correct the ^{10}Be ages for cover by vegetation, but we describe its occurrence and potential influence in detail because most Rwenzori boulders sampled are surrounded by a thick vegetation and/or forest cover (Fig. 2). The moraines we sampled in the Mubuku and Bujuku valleys are located in Montane Forest (1500–2500 m asl), Bamboo (2500–3000 m asl), and Heather/Rapanea (3000–4000 m asl) vegetation zones (Osmaston, 2006). Moraines sampled in the Nyamugasani valley are located in the Heather/Rapanea (3000–4000 m asl) and Alpine (3800–4500 m asl) vegetation zones (Osmaston, 2006). In general, sampled boulders were covered by moss that was ~1–15 cm thick. In some cases, boulders were covered by small shrubs (~1–1.5 m high) and trees (~10–40 cm diameter).

Prior work estimating the impact of vegetation cover on surface-exposure ages used a ‘shredded biomass’ model that assumes a uniform thickness and density of vegetation on a rock surface (Plug et al., 2007; Dunai et al., 2010). The average biomass of mosses in the Rwenzori Montane Forest zone is 0.004–0.25 g/cm^2 (Pentecost, 1998; Osmaston, 2006). We sampled the vegetation and moss cover on a moraine in the Bujuku valley (Mahoma 8 moraine, ~2650 m asl; Fig. 4) and determined a dry weight vegetation density of ~0.02–0.20 g/cm^3. Using the ‘shredded biomass’ model, vegetation cover 0–15 cm thick and of density 0.02–0.25 g/cm^2 atop a boulder would require a reduction of the final ^{10}Be exposure age of ~0–3% (Plug et al., 2007; Dunai et al., 2010). Beyond direct moss or vegetation cover, modeled impacts of temperate boreal or rainforest vegetation on the incoming cosmic ray flux suggest that nuclide production rates may be reduced by ~2–7% in areas of dense forest cover (Plug et al., 2007). The majority of this amelioration is caused by tree stems, although some also comes from shielding by the tree canopy.

Due to the uncertainty of vegetation type and thickness over time, we refrain from correcting the Rwenzori ^{10}Be ages for the potential impacts of vegetation cover. In all three valleys the timing and pattern of forest succession since deglaciation from the LGM is uncertain and the types and thicknesses of vegetation cover on the boulders has likely varied over time due to changes in climate. We note that there is no clear pattern of younger apparent exposure ages with thicker vegetation cover on single moraine forms, suggesting that vegetation does not have a significant impact on the ^{10}Be ages reported over the time scales of consideration in this study (Fig. 3). However, we suggest that any correction would likely reduce the ^{10}Be ages by only a few percent and, therefore, would not alter our overall interpretations.

All previously published ^{10}Be ages referenced in the text are presented as calculated using the same low-latitude, high-altitude production rate (Kelly et al., 2015) and scaling framework (“St” scaling; Lal, 1991; Stone, 2000) we use for the Rwenzori chronology. In addition, all radiocarbon ages are presented in calibrated years before present (cal yr BP) as midpoint (2-sigma uncertainty) ages, calibrated using the IntCa13 radiocarbon curve (Reimer et al., 2013) and Calib 7.1 (Stuiver et al., 2019).

4. Results

All sampled moraines were originally classified as Omurubaho stage deposits by Osmaston (1989), except those in the Mubuku valley and in the Bujuku valley near the Mubuku-Bujuku Rivers’ confluence, which were classified as Lake Mahoma stage deposits. In order to discuss the pattern of deglaciation in individual valleys, we identify each moraine by the name of the valley in which it occurs and a number corresponding to its stratigraphic position relative to other dated moraines in the valley. The innermost (most upvalley) ^{10}Be-dated moraine in any catchment is denoted as moraine ‘0’. All ^{10}Be ages (in yr BP) are shown on maps of the three catchments (Figs. 4–6) with associated internal age uncertainty and are given in Table 1.

4.1. Bujuku valley

In the Bujuku valley, two left-lateral moraine segments, Bujuku 8 and Bujuku 7, occur ~100–300 m upvalley of the Mubuku-Bujuku Rivers’ confluence (Fig. 4). These mark the extent of ice after it had separated from the once-joined Mubuku-Bujuku glacier, which deposited the large Lake Mahoma stage moraines dated to the LGM. The Bujuku 8 and 7 moraine crests vary along their length from sharp and well-defined to rounded and less distinct. The moraines have ~1–5 m relief above the valley wall upon which they occur and are located ~30–50 m above the Bujuku River, which has incised the valley floor. Two samples from the Bujuku 8 moraine yield ^{10}Be

Table 2

^{10}Be sample information. All samples are listed according to valley, landform, sample name, and corresponding map identification number (as in Figs. 4–6). Sample location, elevation, thickness, topographic shielding, and year of sample collection are presented here with calculated ^{10}Be concentrations in atoms/gram quartz.

Map ID	Landform	Sample ID	Latitude (DD)	Longitude (DD)	Elev. (m)	Atm.	Thickness (cm)	Density (g/cm^3)	Shielding	Erosion (mm/yr)	^{10}Be (atoms/g)	$\pm^{10}$Be (atoms/g)	Year collected
Mubuku valley													
1	Mubuku 0	RZ-16-41	0.34533	29.95181	2955	std	1.4	2.65	0.965	0	1.74 E+05	4.32 E+03	2016
2	Mubuku 0	RZ-16-43	0.34547	29.95206	2975	std	2.8	2.65	0.965	0	2.15 E+05	5.37 E+03	2016
3	Mubuku 0	RZ-16-44	0.34543	29.95196	2948	std	2.1	2.65	0.942	0	1.90 E+05	4.90 E+03	2016
Bujuku valley													
4	Bujuku 8	RZ-16-07	0.35942	29.97108	2673	std	2.4	2.65	0.964	0	2.92 E+04	3.80 E+03	2016
5	Bujuku 8	RZ-16-08	0.35855	29.97204	2630	std	2.3	2.65	0.960	0	1.79 E+05	5.20 E+03	2016
6	Bujuku 7	RZ-16-02	0.36100	29.96632	2776	std	2.9	2.65	0.956	0	2.32 E+05	4.32 E+03	2016
7	Bujuku 7	RZ-16-03	0.36040	29.96773	2737	std	1.8	2.65	0.977	0	2.15 E+05	5.20 E+03	2016
8	Bigo Drift	RZ-16-09	0.38174	29.93753	3332	std	2.7	2.65	0.957	0	2.09 E+05	6.46 E+03	2016
9	Bigo Drift	RZ-16-11	0.38177	29.93755	3240	std	2.9	2.65	0.957	0	2.86 E+05	8.55 E+03	2016
10	Bigo Drift	RZ-16-13	0.38180	29.93758	3320	std	1.2	2.65	0.943	0	4.20 E+05	8.35 E+03	2016
11	Bujuku 6	RZ-16-24	0.38550	29.93015	3473	std	1.5	2.65	0.974	0	1.95 E+05	5.44 E+03	2016
12	Bujuku 6	RZ-16-25	0.38540	29.93022	3470	std	1.5	2.65	0.974	0	2.83 E+05	7.30 E+03	2016
13	Bujuku 5	RZ-16-21	0.38590	29.92945	3491	std	2.4	2.65	0.974	0	3.19 E+05	6.91 E+03	2016
14	Bujuku 5	RZ-16-26	0.38500	29.93023	3465	std	1.9	2.65	0.973	0	3.05 E+05	6.40 E+03	2016
15	Bujuku 4	RZ-16-17	0.38381	29.93081	3436	std	3.3	2.65	0.977	0	3.07 E+05	8.06 E+03	2016
16	Bujuku 4	RZ-16-18	0.38370	29.93089	3433	std	2.1	2.65	0.974	0	2.98 E+05	7.98 E+03	2016
17	Bujuku 3	RZ-16-14	0.38148	29.93198	3347	std	4.0	2.65	0.977	0	2.67 E+05	7.91 E+03	2016
18	Bujuku 2	RZ-12-11	0.38679	29.92037	3526	std	1.6	2.65	0.966	0	3.25 E+05	6.14 E+03	2012
19	Bujuku 2	RZ-12-12	0.38679	29.92047	3514	std	0.6	2.65	0.977	0	3.12 E+05	5.91 E+03	2012
20	Bujuku 2	RZ-12-13	0.38622	29.92126	3473	std	0.6	2.65	0.977	0	2.89 E+05	5.46 E+03	2012
	Bujuku 2	RZ-12–13x	0.38622	29.92126	3473	std	0.6	2.65	0.977	0	2.82 E+05	5.32 E+03	2012
21	Bujuku 1	RZ-12-14	0.38660	29.92165	3450	std	1.3	2.65	0.972	0	2.85 E+05	5.97 E+03	2012
22	Bujuku 1	RZ-12-15	0.38670	29.92143	3454	std	0.4	2.65	0.95	0	2.82 E+05	4.61 E+03	2012
23	Bujuku 1	RZ-12-16	0.38667	29.92144	3443	std	0.9	2.65	0.972	0	2.91 E+05	5.67 E+03	2012
24	Bujuku 0	RZ-12-17	0.37908	29.90679	3719	std	0.9	2.65	0.955	0	2.63 E+05	4.98 E+03	2012
25	Bujuku 0	RZ-12-18	0.37927	29.90700	3705	std	0.4	2.65	0.952	0	2.77 E+05	8.51 E+03	2012
26	Bujuku 0	RZ-16-31	0.37900	29.90649	3730	std	2.3	2.65	0.954	0	2.67 E+05	5.26 E+03	2012
27	Bujuku Slide	RZ-16-35	0.37595	29.89511	3913	std	0.8	2.65	0.901	0	2.93 E+05	5.41 E+03	2016
28	Bujuku Slide	RZ-16-36	0.37596	29.89498	3913	std	0.8	2.65	0.931	0	2.70 E+05	5.03 E+03	2016
29	Bujuku Slide	RZ-16-39	0.37576	29.89535	3916	std	1.4	2.65	0.929	0	2.68 E+05	4.99 E+03	2016
Nyamugasani valley													
30	Katunda boulder	RZ-15-05	0.27685	29.89385	3814	std	6.1	2.65	0.976	0	3.31 E+05	6.29 E+03	2015
31	Katunda boulder	RZ-15-06	0.27712	29.89385	3817	std	2.7	2.65	0.976	0	3.32 E+05	5.48 E+03	2015
32	Nyamugasani 2	LA-2	0.29487	29.89638	3871	std	4.0	2.65	0.979	0	2.84 E+05	5.43 E+03	2009
33	Nyamugasani 2	LA-1	0.29488	29.89633	3870	std	1.0	2.65	0.976	0	3.19 E+05	6.94 E+03	2009
	Nyamugasani 2	LA-1x	0.29488	29.89633	3870	std	1.0	2.65	0.976	0	3.08 E+05	9.35 E+03	2009

(*continued on next page*)

Table 2 (*continued*)

Map ID	Landform	Sample ID	Latitude (DD)	Longitude (DD)	Elev. (m)	Atm.	Thickness (cm)	Density (g/cm^3)	Shielding	Erosion (mm/yr)	^{10}Be (atoms/g)	±^{10}Be (atoms/g)	Year collected
34	Nyamugasani 2	LA-3	0.29490	29.89642	3872	std	1.0	2.65	0.979	0	3.15 E+05	5.99 E+03	2009
35	Nyamugasani 2	LA-5	0.29502	29.89685	3968	std	1.4	2.65	0.978	0	3.09 E+05	5.86 E+03	2009
	Nyamugasani 2	LA-5x	0.29502	29.89685	3968	std	1.4	2.65	0.978	0	3.05 E+05	5.01 E+03	2009
36	Nyamugasani 1	RZ-12-33	0.30186	29.89462	3980	std	0.5	2.65	0.987	0	3.09 E+05	5.83 E+03	2012
37	Nyamugasani 1	RZ-12-34	0.30180	29.89468	3974	std	1.0	2.65	0.987	0	3.03 E+05	5.70 E+03	2012
38	Nyamugasani 1	RZ-12-36	0.30214	29.89513	3981	std	1.2	2.65	0.993	0	3.03 E+05	5.70 E+03	2012
39	Nyamugasani 1	RZ-12-37	0.30222	29.89515	3980	std	1.5	2.65	0.993	0	2.99 E+05	6.21 E+03	2012
40	Nyamugasani 0	RZ-12-38	0.30624	29.89303	4007	std	3.5	2.65	0.971	0	3.04 E+05	5.72 E+03	2012
41	Nyamugasani 0	RZ-12-39	0.30551	29.89288	4001	std	0.8	2.65	0.984	0	2.98 E+05	5.62 E+03	2012
42	Nyamugasani 0	RZ-12-41	0.30515	29.89296	4001	std	1.1	2.65	0.983	0	2.99 E+05	5.64 E+03	2012
43	Nyamugasani 0	RZ-12-44	0.30509	29.89175	4013	std	2.0	2.65	0.966	0	2.90 E+05	7.30 E+03	2012
44	Kopello boulder	KOP-1	0.31085	29.89162	4033	std	1.3	2.65	0.992	0	2.87 E+05	7.42 E+03	2009
45	Kopello boulder	KOP-2	0.31108	29.89142	4032	std	2.0	2.65	0.963	0	3.12 E+05	7.62 E+03	2009
46	Kopello boulder	KOP-4A	0.31070	29.89180	4030	std	1.8	2.65	0.963	0	3.20 E+05	8.86 E+03	2009
47	Kopello boulder	KOP-5	0.30958	29.89270	4022	std	3.0	2.65	0.963	0	2.17 E+05	5.34 E+03	2009
48	Kopello boulder	RZ-15-12	0.31107	29.89111	4025	std	2.1	2.65	0.97	0	2.93 E+05	5.59 E+03	2015

ages of 13.9 ± 0.4 ka (RZ-16-08) and 2.2 ± 0.3 ka (RZ-16-07). Immediately upvalley, two samples from the Bujuku 7 moraine yield ^{10}Be ages of 15.4 ± 0.4 ka (RZ-16-03) and 16.8 ± 0.3 ka (RZ-16-02).

The area surrounding Bigo Bog is blanketed by drift (Fig. 5). This drift deposit is identifiable in aerial imagery as a distinct change in vegetation, presumably due to differences in subsurface drainage, and on the ground through the appearance of large (1–3 m high) boulders on the valley floor and walls. The extent of the deposit is delineated in Fig. 5 as late-glacial moraine. Three samples from boulders atop the outermost, downvalley limit of the drift yield ^{10}Be ages of 22.8 ± 0.5, 16.1 ± 0.5, and 11.2 ± 0.4 ka (RZ-16-13, 11, 09). These boulders are not associated with a moraine ridge.

Bigo Bog is bounded by a series of tightly spaced moraines. The Bujuku 6 to Bujuku 3 moraines occur along the bog's more eastern, downvalley limit near where the Bujuku River emerges from the bog and continues to flow downvalley (Fig. 5). These moraines feature sharp crests and have ~10–20 m relief above the bog surface. Two samples from the outermost sampled moraine, Bujuku 6, yield ^{10}Be ages of 13.8 ± 0.4 (RZ-16-25) and 9.5 ± 0.3 ka (RZ-16-24). Immediately inboard of Bujuku 6, two samples from the Bujuku 5 moraine yield a mean age of ~15.2 ± 0.4 ka (RZ-16-21, 26). Inboard of the Bujuku 5 moraine, two samples from the Bujuku 4 moraine yield a mean age of ~15.1 ± 0.4 ka (RZ-16-17, 18). A single sample from a dissected ridge segment on the Bujuku 3 moraine dates to 14.1 ± 0.4 ka (RZ-16-14).

A bedrock knob bisects the valley floor on the western, upvalley edge of Bigo Bog. A series of right-lateral moraines on the northern flank of the knob both abut and plunge into the modern bog surface; these ridges mark the former position of a glacier that flowed from the upper Bujuku valley (Fig. 5). Three samples from one of these lateral moraines (Bujuku 2) yield a mean age of ~14.7 ± 0.8 ka (RZ-12-11, 12, 13). Approximately 30 m below the Bujuku 2 moraine, three samples from the lateral Bujuku 1 moraine yield a mean age of ~14.1 ± 0.2 ka (RZ-12-14, 15, 16). The next preserved moraines in the Bujuku valley occur ~1.5 km upvalley from Bigo Bog, where a cluster of partially preserved lateral moraines marks the most upvalley position of ice in the vicinity. Three samples from a right-lateral (Bujuku 0) moraine yield a mean age of ~11.7 ± 0.4 ka (RZ-12-17, 18; RZ-16-31). We note that no additional moraines occur between the Bujuku 0 moraine and the (estimated) historical-age moraines on the slopes of Mt. Speke and Mt. Stanley (Osmaston, 1989).

In addition to boulders on moraines we dated three boulders on the toe of a landslide deposit near the outlet of Lake Bujuku, roughly 2 km upvalley from the Bujuku 0 moraine (Fig. 5). Two of these samples yield ^{10}Be ages of 11.0 ± 0.2 ka (RZ-16-36, 39) and a third yields a^{10}Be age of 12.4 ± 0.2 ka (RZ-16-35).

4.2. *Mubuku valley*

The left-lateral Mubuku 0 moraine occurs ~2.5 km upvalley of the Mubuku and Bujuku Rivers' confluence and is the innermost moraine within a sequence of moraines in the Mubuku valley (Fig. 4). The crest of the moraine is well-defined, undulatory and has roughly 10 m relief above the valley floor. The ice-contact moraine slope is steep and may have been partially eroded by the Mubuku River. Three samples collected from the Mubuku 0 moraine yield ^{10}Be ages of 11.2 ± 0.3, 13.8 ± 0.3, and 12.6 ± 0.3 ka (RZ-16-41, 43, 44).

4.3. *Nyamugasani valley*

In the Nyamugasani valley, two boulders on a bedrock rise that dams Lake Katunda yield ^{10}Be ages of 14.1 ± 0.3 (RZ-15-05) and

Table 3

^{10}Be sample chemistry. Samples are listed according to valley, landform, sample name, and corresponding map identification number (as in Figs. 4–6). Quartz weight, beryllium-9 carrier weight added to each sample, beryllium-9 carrier concentration, the sample ^{10}Be/^{9}Be ratio, and the process blank ^{10}Be/^{9}Be ratio are included here. All ^{10}Be/^{9}Be ratios were measured at Lawrence Livermore National Laboratory Center for Mass Spectrometry (CAMS) and normalized to the 07KNSTD3110 standard (Nishiizumi et al., 2007).

Map ID	Landform	Sample ID	Cathode ID	Quartz (g)	Carrier wt. (g)	Carrier Conc. (ppm)	Sample (^{10}Be/^{9}Be)	± Sample (^{10}Be/^{9}Be)	Process Blank Cathode ID	Blank (^{10}Be/^{9}Be)	± Blank (^{10}Be/^{9}Be)
Mubuku valley											
1	Mubuku 0	RZ-16-41	BE43141	3.1667	0.1548	1349	3.959E-14	9.796E-16	BE43147	5.689E-16	1.274E-16
2	Mubuku 0	RZ-16-43	BE43142	3.0083	0.1576	1349	4.551E-14	1.137E-15	BE43147	5.689E-16	1.274E-16
3	Mubuku 0	RZ-16-44	BE43143	3.0327	0.1562	1349	4.096E-14	1.056E-15	BE43147	5.689E-16	1.274E-16
Bujuku Valley											
4	Bujuku 8	RZ-16-07	BE42145	5.1013	0.3499	1344	4.738E-15	6.177E-16	BE42147	6.176E-16	5.124E-16
5	Bujuku 8	RZ-16-08	BE42146	5.0411	0.1547	1344	6.491E-14	1.887E-15	BE42147	6.176E-16	5.124E-16
6	Bujuku 7	RZ-16-02	BE42143	5.0669	0.2008	1344	6.529E-14	1.213E-15	BE42147	6.176E-16	5.124E-16
7	Bujuku 7	RZ-16-03	BE42144	5.0408	0.1976	1344	6.102E-14	1.476E-15	BE42147	6.176E-16	5.124E-16
8	Bigo Drift	RZ-16-09	BE43561	2.0904	0.2040	973	6.792E-16	2.579E-16	BE43567	6.792E-16	2.579E-16
9	Bigo Drift	RZ-16-11	BE43562	2.0968	0.2034	973	6.792E-16	2.579E-16	BE43567	6.792E-16	2.579E-16
10	Bigo Drift	RZ-16-13	BE43563	2.1483	0.2039	973	6.792E-16	2.579E-16	BE43567	6.792E-16	2.579E-16
11	Bujuku 6	RZ-16-24	BE43569	2.1943	0.2014	973	3.275E-14	9.116E-16	BE43573	4.475E-16	1.317E-16
12	Bujuku 6	RZ-16-25	BE43570	2.2332	0.1996	973	4.878E-14	1.256E-15	BE43573	4.475E-16	1.317E-16
13	Bujuku 5	RZ-16-21	BE43568	2.2553	0.1988	973	5.567E-14	1.206E-15	BE43573	4.475E-16	1.317E-16
14	Bujuku 5	RZ-16-26	BE43571	2.1882	0.1999	973	5.129E-14	1.078E-15	BE43573	4.475E-16	1.317E-16
15	Bujuku 4	RZ-16-17	BE43565	2.0313	0.2040	973	6.792E-16	2.579E-16	BE43567	6.792E-16	2.579E-16
16	Bujuku 4	RZ-16-18	BE43566	2.0427	0.2043	973	6.792E-16	2.579E-16	BE43567	6.792E-16	2.579E-16
17	Bujuku 3	RZ-16-14	BE43564	2.0240	0.2038	973	6.792E-16	2.579E-16	BE43567	6.792E-16	2.579E-16
18	Bujuku 2	RZ-12-11	BE36868	6.3178	0.1622	1328	1.427E-13	2.696E-15	BE36874	3.833E-16	1.416E-16
19	Bujuku 2	RZ-12-12	BE36869	4.8772	0.1628	1328	1.053E-13	1.994E-15	BE36874	3.833E-16	1.416E-16
20	Bujuku 2	RZ-12-13	BE37992	8.0182	0.1629	1335	1.597E-13	3.015E-15	BE37998	4.378E-16	1.493E-16
	Bujuku 2	RZ-12–13x	BE41130	8.4586	0.1639	1341	1.623E-13	3.064E-15	BE41134	8.484E-16	2.320E-16
21	Bujuku 1	RZ-12-14	BE36870	3.3612	0.1613	1328	6.689E-14	1.401E-15	BE36874	3.833E-16	1.416E-16
22	Bujuku 1	RZ-12-15	BE36871	6.0607	0.1629	1328	1.183E-13	1.935E-15	BE36874	3.833E-16	1.416E-16
23	Bujuku 1	RZ-12-16	BE37993	4.4068	0.1627	1335	8.830E-14	1.722E-15	BE37998	4.378E-16	1.493E-16
24	Bujuku 0	RZ-12-17	BE36872	6.7221	0.1623	1328	1.228E-13	2.323E-15	BE36874	3.833E-16	1.416E-16
25	Bujuku 0	RZ-12-18	BE36873	4.7221	0.163	1328	9.053E-14	2.778E-15	BE36874	3.833E-16	1.416E-16
26	Bujuku 0	RZ-16-31	BE43572	3.1557	0.1996	973	6.491E-14	1.278E-15	BE43573	4.475E-16	1.317E-16
27	Bujuku Slide	RZ-16-35	BE42269	30.226	0.1997	1345	4.934E-13	9.113E-15	BE42272	1.510E-15	2.046E-16
28	Bujuku Slide	RZ-16-36	BE42270	26.1295	0.2022	1345	3.885E-13	7.227E-15	BE42272	1.510E-15	2.046E-16
29	Bujuku Slide	RZ-16-39	BE42271	22.0332	0.2021	1345	3.257E-13	6.051E-15	BE42272	1.510E-15	2.046E-16
Nyamugasani Valley											
30	Katunda boulder	RZ-15-05	BE39120	4.083	0.1650	1335	9.175E-14	1.745E-15	BE39123	1.129E-15	2.180E-16
31	Katunda boulder	RZ-15-06	BE39121	4.103	0.1628	1335	9.389E-14	1.548E-15	BE39123	1.129E-15	2.180E-16
32	Nyamugasani 2	LA-2	BE30979	6.5752	0.1989	1030	1.365E-13	2.609E-15	BE30980	3.602E-16	1.092E-16
33	Nyamugasani 2	LA-1	BE33734	6.0074	0.1623	1318	1.342E-13	2.918E-15	BE33740	2.873E-16	1.109E-16
	Nyamugasani 2	LA-1x	BE41126	8.113	0.1615	1341	1.724E-13	5.243E-15	BE41134	8.484E-16	2.320E-16
34	Nyamugasani 2	LA-3	BE33735	6.0693	0.1554	1318	1.396E-13	2.659E-15	BE33740	2.873E-16	1.109E-16
35	Nyamugasani 2	LA-5	BE33736	6.0111	0.1617	1318	1.305E-13	2.474E-15	BE33740	2.873E-16	1.109E-16
	Nyamugasani 2	LA-5x	BE41127	8.2705	0.1644	1341	1.712E-13	2.815E-15	BE41134	8.484E-16	2.320E-16
36	Nyamugasani 1	RZ-12-33	BE34160	6.1051	0.1634	1319	1.311E-13	2.473E-15	BE34168	4.070E-16	1.436E-16
37	Nyamugasani 1	RZ-12-34	BE34161	6.0271	0.1625	1319	1.276E-13	2.398E-15	BE34168	4.070E-16	1.436E-16
38	Nyamugasani 1	RZ-12-36	BE34162	6.005	0.1627	1319	1.267E-13	2.385E-15	BE34168	4.070E-16	1.436E-16
39	Nyamugasani 1	RZ-12-37	BE34163	6.0069	0.1624	1319	1.253E-13	2.604E-15	BE34168	4.070E-16	1.436E-16
40	Nyamugasani 0	RZ-12-38	BE34164	6.0051	0.1631	1319	1.271E-13	2.387E-15	BE34168	4.070E-16	1.436E-16
41	Nyamugasani 0	RZ-12-39	BE34165	6.0051	0.1633	1319	1.242E-13	2.344E-15	BE34168	4.070E-16	1.436E-16
42	Nyamugasani 0	RZ-12-41	BE34166	6.1877	0.1633	1319	1.286E-13	2.423E-15	BE34168	4.070E-16	1.436E-16
43	Nyamugasani 0	RZ-12-44	BE34167	6.0497	0.1631	1319	1.222E-13	3.071E-15	BE34168	4.070E-16	1.436E-16
44	Kopello boulder	KOP-1	BE30978	6.5625	0.1961	1030	1.396E-13	3.609E-15	BE30980	3.602E-16	1.092E-16
45	Kopello boulder	KOP-2	BE33737	6.018	0.1619	1318	1.316E-13	3.216E-15	BE33740	2.873E-16	1.109E-16

(*continued on next page*)

Table 3 (*continued*)

Map ID	Landform	Sample ID	Cathode ID	Quartz (g)	Carrier wt. (g)	Carrier Conc. (ppm)	Sample (^{10}Be/^{9}Be)	± Sample (^{10}Be/^{9}Be)	Process Blank Cathode ID	Blank (^{10}Be/^{9}Be)	± Blank (^{10}Be/^{9}Be)
46	Kopello boulder	KOP-4A	BE33738	6.034	0.1614	1318	1.359E-13	3.763E-15	BE33740	2.873E-16	1.109E-16
47	Kopello boulder	KOP-5	BE33739	6.0837	0.1616	1318	9.292E-14	2.285E-15	BE33740	2.873E-16	1.109E-16
48	Kopello boulder	RZ-15-12	BE39122	4.004	0.1637	1335	8.038E-14	1.533E-15	BE39123	1.129E-15	2.180E-16

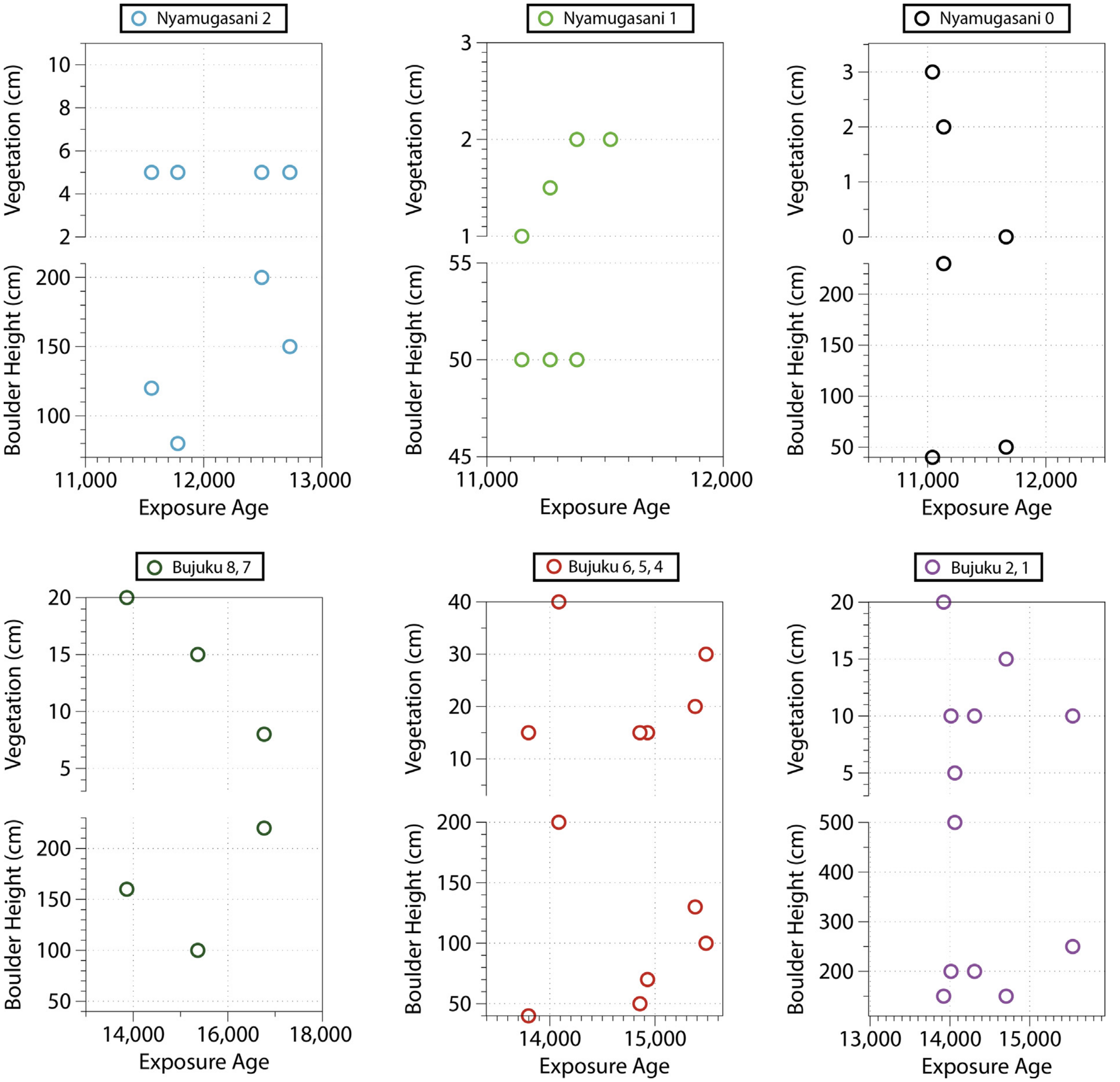

Fig. 3. Individual beryllium-10 exposure ages from Rwenzori moraines plotted versus vegetation thickness in cm (top) and boulder height (bottom). All data are color coded by individual moraines or, where moraines are in close geographic proximity, by moraine group.

13.8 ± 0.2 ka (RZ-15-06)(Fig. 6). Approximately two kilometers upvalley from Lake Katunda, the upper Nyamugasani valley features a sequence of moraine ridges, some of which dam lakes. Lake Africa is dammed by the most downvalley of these moraines, which we term the Nyamugasani 2 moraine. This moraine occurs at a constriction in the valley, has ~1–2 m relief above the valley floor, and features a single rounded crest. Four samples from the moraine yield ^{10}Be ages of 11.6 ± 0.2 (LA-2), 11.8 ± 0.2 (LA-5), 12.7 ± 0.3 (LA-1) and 12.5 ± 0.3 ka (LA-3). These ages provide a mean moraine age of ~12.1 ± 0.6 ka.

Roughly 1 km upvalley from the Nyamugasani 2 moraine, the Nyamugasani 1 moraine has ~5 m relief above the valley floor and features a sharp crest (Fig. 6). Four samples from this moraine ridge yield a mean age of ~11.3 ± 0.2 ka (RZ-12-33, 34, 36, 37). Inboard of the Nyamugasani 1 moraine, Lake Bigata is dammed by the Nyamugasani 0 moraine. The Nyamugasani 0 moraine is similar in form

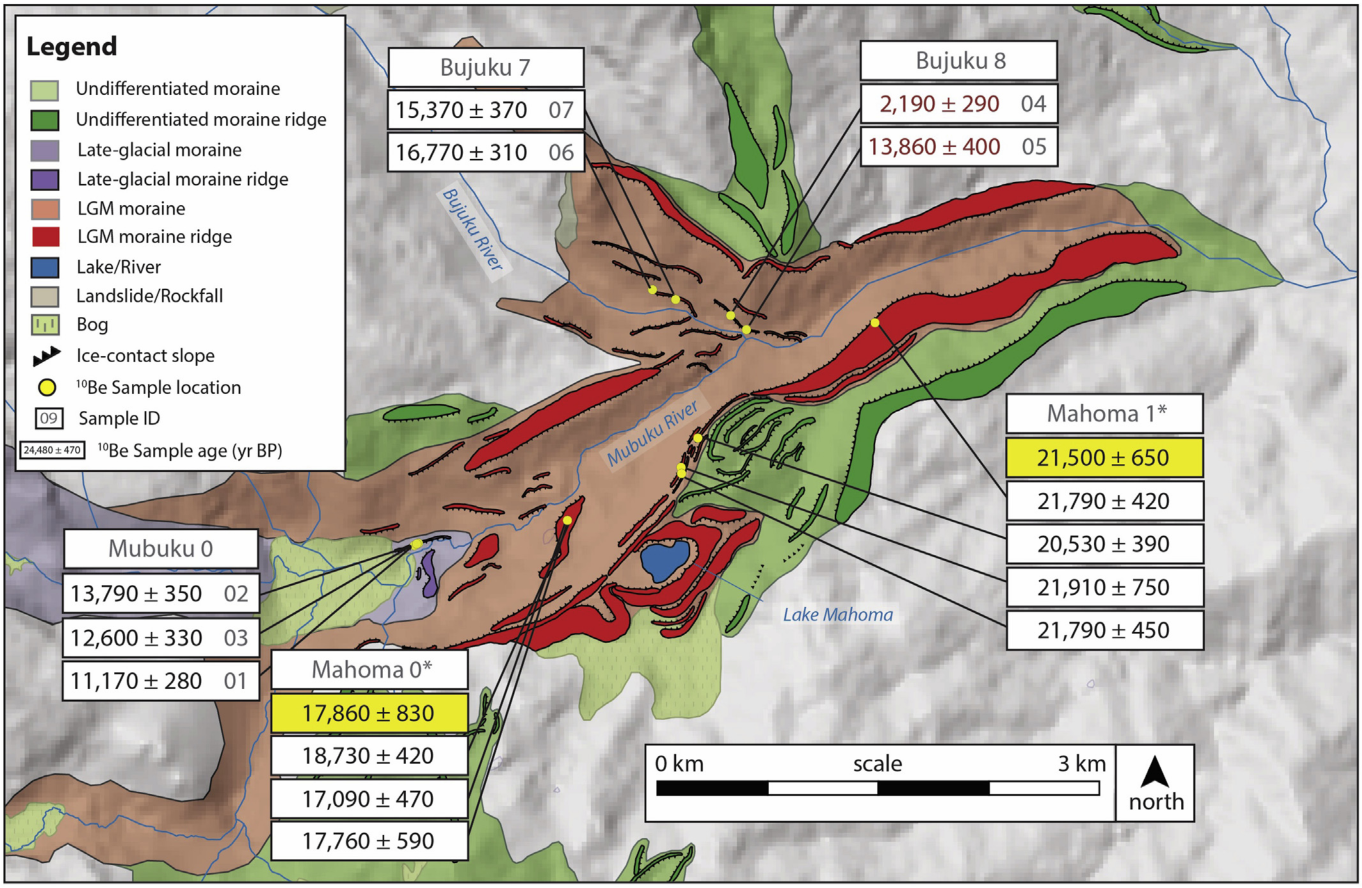

Fig. 4. Glacial-geomorphic map of the Mubuku and lower Bujuku valleys and ^{10}Be ages as reported in Table 1. Ages we consider to be affected by post-depositional processes are shown in red. Arithmetic-mean moraine ages are boxed in yellow. Sample ID numbers as in Tables 1–3 are in grey. ^{10}Be ages from the Mahoma 0 (Jackson et al., 2019) and Mahoma 1 (Kelly et al., 2014) moraines are also shown and are marked with an asterisk.

to the Nyamugasani 1 moraine with ~5 m relief above the valley floor. Four samples from the Nyamugasani 0 moraine yield a mean age of ~11.2 ± 0.2 ka (RZ-12-38, 39, 41, 44).

There are no moraines preserved upvalley of the Nyamugasani 0 moraine although numerous boulders occur on the valley floor. Approximately 0.5 km upvalley from Lake Bigata, Lake Kopello is dammed by a bedrock rise that transits the valley floor. Five samples from boulders on this bedrock rise yield ^{10}Be ages of 10.5 ± 0.3 (KOP-1), 11.8 ± 0.3 (KOP-2), 12.1 ± 0.3 (KOP-4A), 8.3 ± 0.2 ka (KOP-5) and 11.0 ± 0.2 ka (RZ-15-12)(Fig. 6).

5. Discussion

5.1. Rwenzori ice extents during the last glacial termination

Deglaciation from the LGM glacial extents in the Rwenzori began at ~21.5 ka (Kelly et al., 2014). Formerly conjoined ice from the Mubuku and Bujuku catchments separated by at least ~17.9 ka (Jackson et al., 2019). In the Bujuku valley, ice retreated ~3 km upvalley of the ~21.5 ka position and ~300 m upvalley of the Mubuku-Bujuku river confluence by ~16.8–15.4 ka, as indicated by ages of the Bujuku 7 moraine. Ice then retreated an additional ~8 km upvalley to the position of the Bujuku 4 and 5 moraines near Bigo Bog by ~15.0 ka. Together, these data indicate that between ~21.5 and 15.0 ka the glacier in the Bujuku valley retreated ~11 km, an ~54% reduction in the glacier's length relative to its LGM maximum extent (Fig. 7).

Whether the slowdown in glacial retreat at ~15–14 ka marked by the Bujuku 4 and 5 moraines near Bigo Bog was influenced primarily by topography is unclear. Bigo Bog is a depression at the confluence of multiple catchments and it is possible that the overdeepened reach may have encouraged the stagnation and stillstand of the ice margin. Because the dated Bujuku 2 and 1 moraines are lateral moraines that terminate in the modern bog, the position of the glacier terminus at ~14.7–14.1 ka is uncertain. However, the position and ages of the Bujuku 2 and 1 moraines indicate that the glacier thinned between ~15 and 14 ka before fully retreating from Bigo Bog at ~14 ka (Figs. 5 and 7).

There are no moraines preserved on the valley floor between the Bujuku 1 moraine (~14.1 ka) and the Bujuku 0 moraine (~11.7 ka) located ~1.5 km upvalley. After ~11.7 ka glacial recession in the valley is constrained by the occurrence of an undisturbed rockfall deposit ~1.5 km upvalley of the Bujuku 0 moraine. The rockfall transits the valley floor and dates to ~11.0 ka ($n = 2$). One sample from the toe of the rockfall yields an age of 12.4 ± 0.2 ka (RZ-16-35), out of stratigraphic order with the dated Bujuku 0 moraine downvalley. We suggest that this age likely results from inherited ^{10}Be within the rock surface. The lobate and undisturbed form of the rockfall suggests that it was free to travel unimpeded. Therefore the rockfall site was ice free at the time of deposition and the Bujuku glacier was upvalley of the rockfall by at least ~11.0 ka.

In the Mubuku valley, although the age of the Mubuku 0 moraine is uncertain, the available data indicate that ice retreated at least an additional kilometer upvalley from its ~17.9 ka extent by

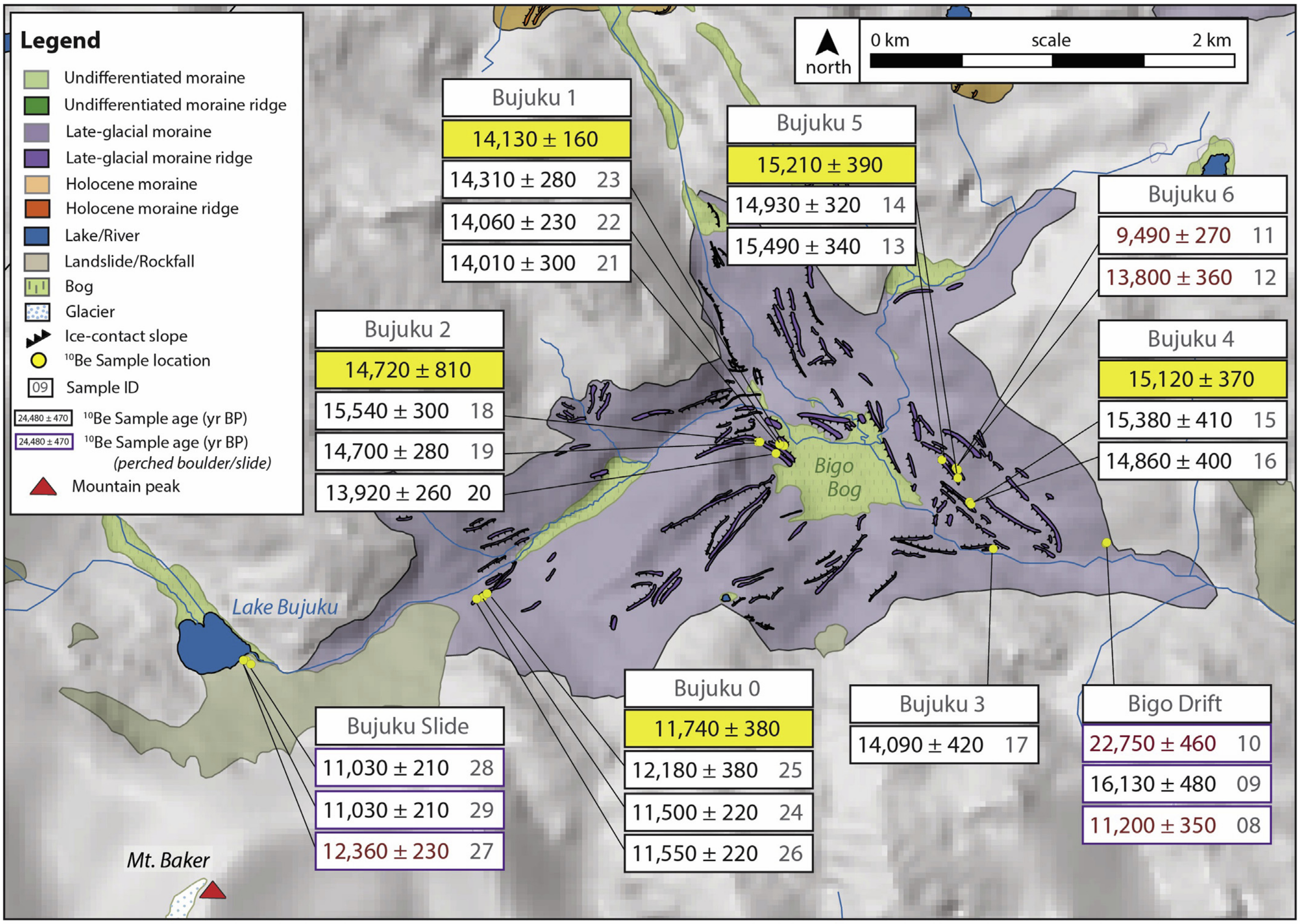

Fig. 5. Glacial-geomorphic map of the Bujuku valley and ^{10}Be ages as reported in Table 1. The area surrounding Bigo Bog is bounded by moraine ridges that delineate the former extent of glaciers fed from multiple catchments. ^{10}Be ages include boulders on moraines (boxed in black) and boulders on bedrock (boxed in purple). Three samples from the toe of a landslide at the outlet of Lake Bujuku are also included (boxed in purple). Ages we consider to be affected by post-depositional processes or to contain inherited ^{10}Be are shown in red. Arithmetic-mean moraine ages are boxed in yellow. Sample ID numbers as in Tables 1–3 are in grey.

~14-11 ka (Jackson et al., 2019, Fig. 7). This retreat is consistent with the glacial chronology inferred from the Bujuku valley described above.

In the Nyamugasani valley, two boulders on bedrock near the outlet of Lake Katunda indicate that ice had retreated ~6.8 km upvalley from outermost mapped Lake Mahoma stage moraines by ~14 ka, an ~54% reduction in the glacier's length relative to its estimated LGM maximum extent (Fig. 7). Two kilometers upvalley from the Katunda boulders, four samples from the Nyamugasani 2 moraine show a bimodal age population. It is possible that the two older ^{10}Be ages (~12.7 and 12.5 ka) are a result of inherited ^{10}Be, or that the two younger ^{10}Be ages (~11.8 and 11.6 ka) reflect post-depositional exhumation or movement of the boulders. The consistency of ages in both the older and younger samples, however, may counter either interpretation. Conservatively, we suggest that ice was at the Nyamugasani 2 moraine position by ~12.6 ka and that ice had abandoned the moraine by ~11.6 ka. After ~11.6 ka, ice retreated upvalley and deposited the Nyamugasani 1 and 0 moraines at ~11.3 and ~11.2 ka, respectively. Moraine deposition ceased in the Nyamugasani valley after ~11.2 ka. The boulders on the bedrock ridge that dams Lake Kopello yield scattered ^{10}Be ages ranging from ~12 to 8 ka. Some of these ages, which are out of stratigraphic order with the dated moraines downvalley, may reflect inherited ^{10}Be in the sample surfaces. We interpret the Kopello ages to indicate continued ice thinning or recession past this location after ~11.2 ka.

Overall, the Rwenzori glacial chronology indicates coherent ice recession in multiple catchments during the last glacial termination. Deglaciation from the LGM was underway by ~21.5 ka (Kelly et al., 2014; Jackson et al., 2019). By ~15–14 ka glaciers in the Bujuku and Nyamugasani valleys had retreated by more than 50% relative to their LGM maximum extents. Recession continued after ~15–14 ka, albeit at a slower net rate. Glaciers then retreated rapidly after ~11.7 ka. A primary implication of these results is that Rwenzori glaciers retreated significantly during HS1. Glacial fluctuations during the subsequent B-A/ACR and YD are less clear, but indicate a slower rate of glacial recession than during HS1 followed by rapid early Holocene retreat.

5.2. Tropical glacial fluctuations during the last glacial termination

Records of glacial fluctuations elsewhere in the tropics, both in Africa and South America, show patterns of deglaciation broadly similar to that in the Rwenzori. On Mt. Elgon in eastern Uganda, two radiocarbon ages from Lake Kilimili (4150 m asl) indicate glacial recession prior to ~12.9–12.6 cal kyr BP (Hamilton and Perrott, 1978). On Mt. Bada in the Arsi Mountains in Ethiopia, a minimum-limiting radiocarbon age from a bog at ~4130 m asl

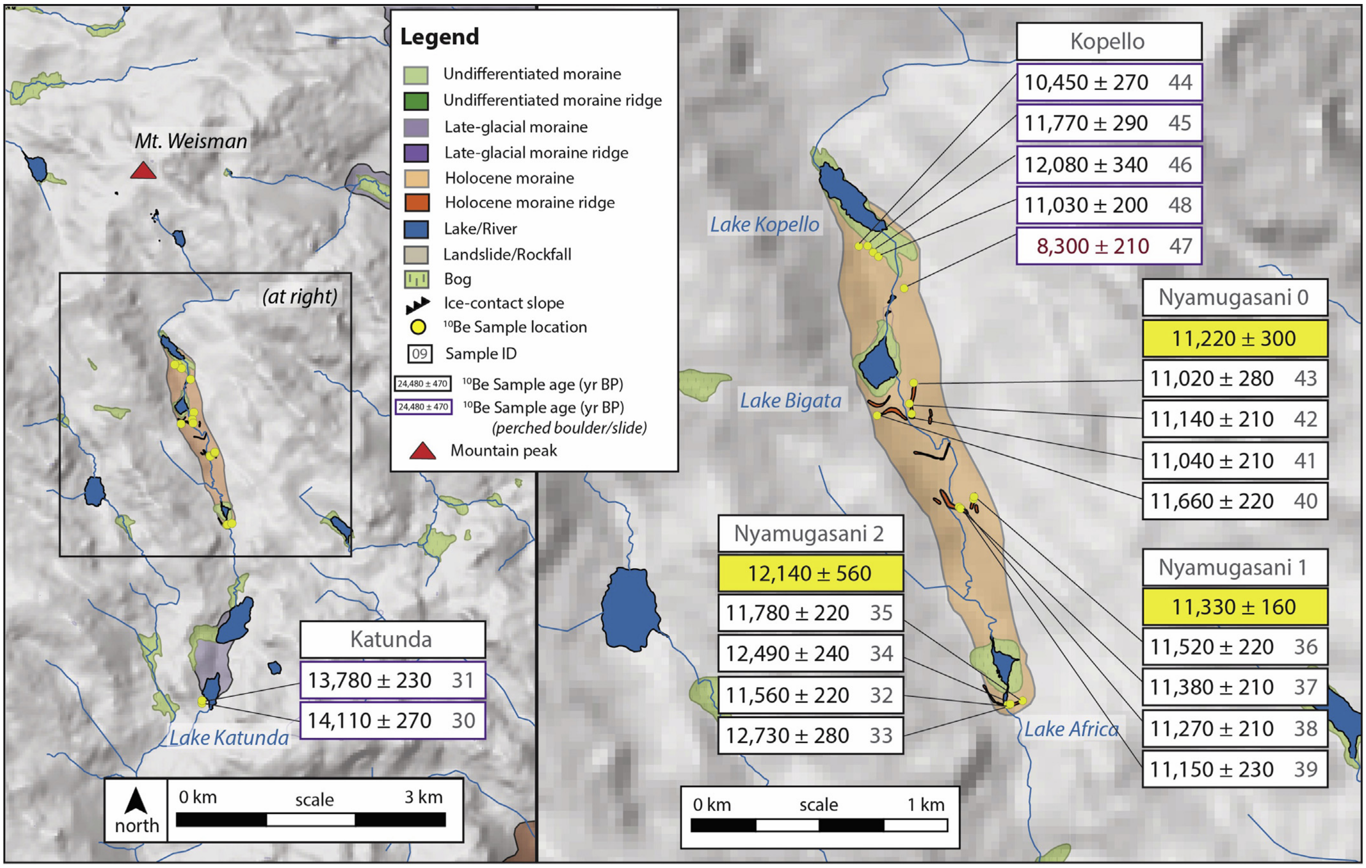

Fig. 6. Glacial-geomorphic map of the Nyamugasani valley and ^{10}Be ages as reported in Table 1. The valley trends southward from the peak of Mt. Weisman (left). In the upper reach of the valley are numerous lakes, some of which are dammed by moraines (right). Samples from the Nyamugasani valley include boulders on moraines (boxed in black) and boulders on bedrock (boxed in purple). Ages we consider to be affected by post-depositional processes are shown in red. Arithmetic-mean moraine ages are boxed in yellow. Sample ID numbers as in Tables 1–3 are in grey.

indicates glacial recession prior to ~13.3 cal kyr BP (Hamilton, 1982). Sediments from Lake Garba Guacha (~3950 m asl) in the Bale Mountains, Ethiopia, indicate that deglaciation from the LGM was underway by at least ~17 cal kyr BP (Tiercelin et al., 2008). High sedimentation rates in Garba Guacha between ~13.4 and 12.5 cal kyr BP are interpreted to reflect increased glacial melt, although this signal may be complicated by bank or slope destabilization or changes in vegetation. Glacier-derived sediment input to the lake decreased after ~12.5 cal kyr BP and the catchment was ice free by ~11.8 cal kyr BP (Tiercelin et al., 2008). Recent chlorine-36 (^{36}Cl) surface-exposure dating of moraines in the Bale Mountains suggests that glaciers in the Harcha and Wasama Valleys retreated during portions of HS1 (Ossendörf et al., 2019). In the Harcha Valley, two 'Stage II' moraines date to ~17.1 ± 0.8 ka ($n = 2$) and ~16.6 ± 2.1 ka ($n = 3$), respectively. Inboard of these 'Stage II" moraines, two 'Stage III' moraine segments yield ages of ~16.3 ± 1.4 ka ($n = 3$) and ~15.3 ± 0.3 ka ($n = 3$). In the Wasama Valley, one 'Stage II' moraine dates to ~17.5 ± 0.9 ka ($n = 3$). Farther upvalley, one 'Stage III' moraine yields an age of ~14.2 ± 0.3 ka ($n = 3$). In both the Wasama and Harcha Valleys there are no dated moraines inboard of the 'Stage III' deposits.

On Kilimanjaro in Tanzania, ^{36}Cl ages from a left-lateral moraine on the south-facing slope of Mawenzi peak yield a mean age of 17.3 ± 2.9 ka ($n = 7$)(Shanahan and Zreda, 2000). Inboard of this moraine, a suite of 3–4 nested moraines yield a mean age of 15.8 ± 2.5 ka ($n = 12$). A second group of samples from a lateral moraine on the eastern flank of Kibo peak are dated at 13.9 ± 2.3 ka ($n = 4$). On Mt. Kenya, two samples from a lateral moraine in the lower Gorges Valley yield a mean ^{36}Cl age of 14.7 ± 1.1 ka, and three samples upvalley yield a mean age of 13.0 ± 1.9 ka (Shanahan and Zreda, 2000). For comparison with the ^{36}Cl ages on Mt. Kenya, minimum-limiting radiocarbon ages of these moraines indicate deposition by 15.2 ± 1.2 cal kyr BP (Mahaney, 1982), within uncertainty of the ^{36}Cl ages. We note, however, that there are undated moraines on Kilimanjaro and Mt. Kenya both downvalley and upvalley of dated deposits.

In summary, prior glacial extent records from East Africa suggest that recession from the LGM maximum glacial extents was underway by at least ~17 ka and that readvances or standstills occurred between ~15 and 13 ka. In catchments where data are available, glaciers were apparently more extensive during the early B-A/ACR than during the YD. However, due to both the low numbers of dated landforms and the resolution of dating techniques employed, there is not sufficient resolution in the existing data to resolve the precise timing of glacial fluctuations at all sites.

Outside of tropical Africa, most prior work on the timing and magnitude of past tropical glacial fluctuations has been conducted in South America. In order to make a direct comparison between Rwenzori and tropical South American glacial chronologies we choose to focus our discussion on prior work that applied ^{10}Be dating of glacial deposits (rather than deposits dated using radiocarbon or other cosmogenic nuclides). We report South American ^{10}Be ages as calculated using the same production rate (Kelly et al., 2015) and scaling scheme ("St"; Lal, 1991; Stone, 2000) as we use for the Rwenzori chronology. Based on our review of prior work, deglaciation in the South American tropics initiated by ~20-19 ka

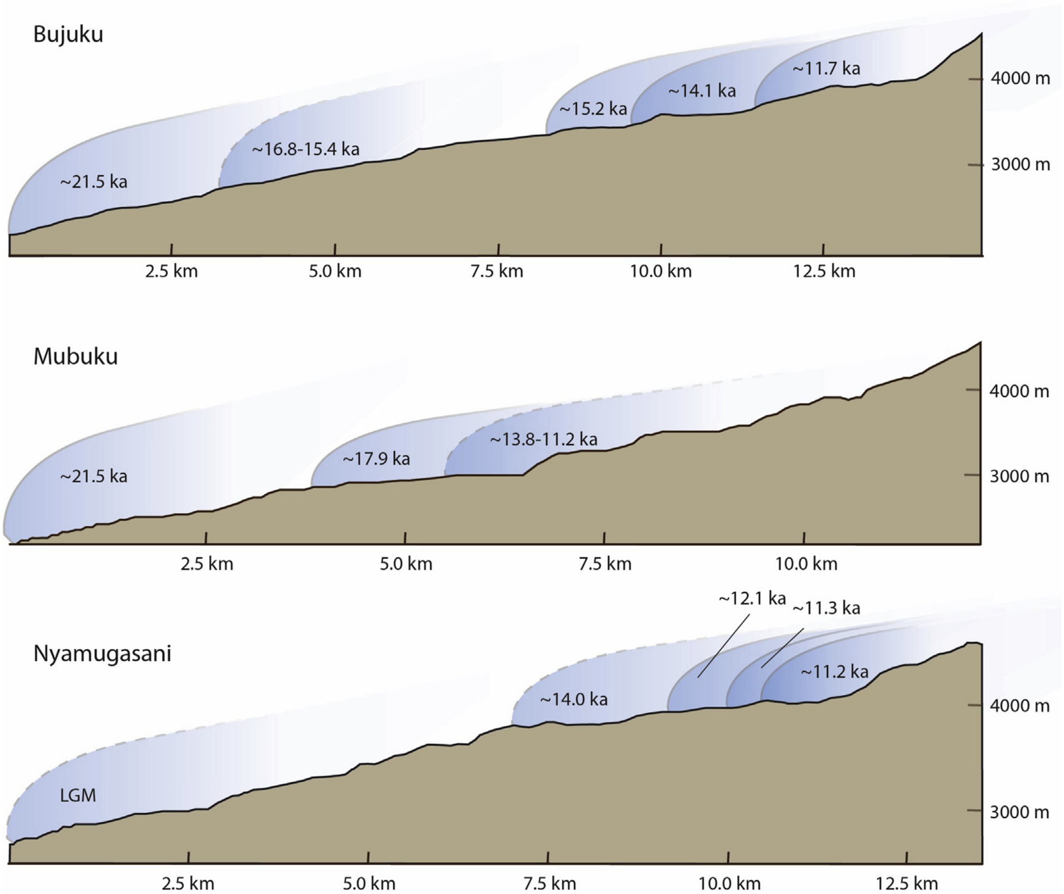

Fig. 7. Changes in glacial extents in the Bujuku, Mubuku, and Nyamugasani catchments during the last glacial termination. Dashed lines indicate inferred ice extents where ^{10}Be ages of a moraine have scatter (e.g., on the Mubuku 0 moraine) or are of boulders on bedrock (e.g., the Katunda boulders in the Nyamugasani valley). Distance downvalley is plotted from the valley headwall relative to the dated or inferred LGM maximum extent (undated in the Nyamugasani valley, also dashed) as measured along the (inferred) central glacier flowline. Plots are drawn onto a 90-m DEM for each catchment. Elevation (m asl) is given individually for each catchment on the right-hand side of the plots.

and continued during HS1, with glaciers retreating by ~30–60% relative to their LGM maximum extents by ~14 ka (e.g., Shakun et al., 2015; Bromley et al., 2016). We note that glaciers in both the northern and southern South American tropics underwent temporally coherent changes during deglaciation (Jomelli et al., 2014; Bromley et al., 2016). There are several moraines dated to between ~14 and 12 ka (Jomelli et al., 2014, 2017), and existing chronologies show that net glacial recession slowed during this interval relative to the rate of net recession during HS1 (Mark et al., 2017; Jomelli et al., 2017). Although glaciers in tropical South America did not retreat markedly between ~14 and 12 ka, glaciers in the region were apparently more extensive during at least some of the B-A/ACR than during the YD (Jomelli et al., 2014; Stansell et al., 2017). After ~12–11 ka, glaciers largely receded to near or within their late-Holocene extents (Jomelli et al., 2014; Mark et al., 2017).

We suggest that the ^{10}Be chronologies from the Rwenzori, elsewhere in tropical Africa, and tropical South America show evidence, to a first order, of temporally similar glacial fluctuations during the last glacial termination. Specifically, these data show that glaciers across the tropics retreated during HS1 and that retreat rates slowed at ~15–14 ka. After ~11 ka glaciers again retreated more rapidly, in many cases to near or within their late-Holocene extents. We note that not all sites feature dated landforms that span the last deglaciation, so the precise timing and phasing of millennial-scale glacial fluctuations across the tropics is yet unknown. Although the existing data are not of the resolution necessary for precise correlation of the glacial chronologies with discrete millennial-scale climate events, the results presented here and prior work discussed above suggest a broad similarity in glacial extent changes across the tropics during the last glacial termination. These results also highlight target areas for continued future efforts to reconstruct and refine past glacial fluctuations.

5.3. Drivers of tropical glacial fluctuations during the last glacial termination

The apparent similarity of glacial fluctuations in tropical Africa and South America, particularly the marked retreat of ice during HS1, suggests that low-latitude glaciers on both continents may have responded to a common forcing mechanism during the last glacial termination. Temperature and precipitation are primary factors that control glacial mass balance (Kaser and Osmaston, 2002) and are the main paleoclimate variables to consider in establishing the drivers of past tropical glacial fluctuations. The regional coherence of tropical South American glacial fluctuations during the last deglaciation in spite of regionally variable precipitation has been noted by previous studies (e.g., Mark et al., 2017) and used to argue for temperature rather than precipitation as the primary control on tropical glacial mass balance (Jomelli et al., 2014; Bromley et al., 2016). Recent investigation of modern Rwenzori glaciers leaves unsettled the question of whether air temperature (Taylor et al., 2006) or humidity (Mölg et al., 2003a) dominated mass balance over the last century, although humidity appears to have been an important and perhaps dominant factor at higher elevation East African sites (i.e., Kilimanjaro; Mölg et al., 2003b). Below we review temperature and precipitation records from tropical Africa and South America, examine the pan-tropical pattern of paleoclimate conditions, and relate these to tropical glacial fluctuations.

Two branched glycerol dialkyl glycerol tetraether (brGDGT) paleotemperature records from alpine lakes on Mt. Kenya, 800 km east of the Rwenzori (Fig. 1), provide estimates of high-elevation temperature that can be compared directly with Rwenzori glacial fluctuations (Fig. 8). These records show marked warming during HS1, an interval of more subdued warming after ~15–14 ka, and temperatures near pre-industrial values by ~11 ka (Loomis et al., 2012, 2017). The Rwenzori glacial chronology generally follows the same pattern with significant glacial recession during HS1, a period of less rapid (net) recession between ~15 and 11 ka, and rapid recession after ~11 ka. However, tropical African brGDGT-based paleotemperature records from the wider region do not show a unified signal of temperature change during the HS1, B-A/ACR and YD (i.e., Powers et al., 2005; Weijers et al., 2007; Tierney et al., 2008; Loomis et al., 2017).

Empirical orthogonal function analyses of African precipitation records and climate model experiments indicate that sites to the north, south, west, and east of the Rwenzori experienced similar precipitation regimes during the last glacial termination (Otto-Bliesner et al., 2014). Therefore, we suggest that the Rwenzori likely experienced precipitation changes similar in sign and timing to this broader pattern. Across tropical Africa, a relatively dry LGM was followed by intensified aridity during HS1, indicated by records of soil acidity and geochemical lake sediment analyses (Weijers et al., 2007; Tierney et al., 2008), as well as by the complete desiccation of Lake Victoria (Gasse, 2000 and citations therein)(Fig. 9). Lake Albert, ~85 km north of the Rwenzori, also records arid conditions during HS1 (Buening et al., 1997; Berke et al., 2014). Glacial recession in the Rwenzori and elsewhere in East Africa during HS1 was coincident with this regional aridity (Ossendörf et al., 2019; Shanahan and Zreda, 2000; Tiercelin et al., 2008). Precipitation in the African tropics increased near the end of HS1 at ~15–14.5 ka (Otto-Bliesner et al., 2014) followed by relative aridity during the YD at Lake Albert (Buening et al., 1997; Berke et al., 2014). The Rwenzori Bujuku 4 and 5 moraines indicate a pause in ice recession at or just before ~15.2 ka, roughly coincident with this increase in precipitation (Gasse, 2000)(Figs. 7–9). Although the deposition of the Bukuju 4 and 5 moraines may, in part, be due to valley topography (Section 5.1.), moraines of similar age in Ethiopia (Ossendörf et al., 2019) and on Mt. Kenya (Shanahan and Zreda, 2000) suggest a regional pattern of glacial fluctuations likely influenced by climate, possibly the increase in precipitation at ~15 ka (Powers et al., 2005; Tierney et al., 2008). We note, however, that glacial recession in the Rwenzori and Bale Mountains (Ossendörf et al., 2019), and perhaps on Kilimanjaro and Mt. Kenya (Shanahan and Zreda, 2000), continued after ~15 ka although precipitation remained elevated. After a period of aridity during the YD, a rapid return to wet conditions at ~11.6 ka marked the onset of the African Humid Period (AHP), an interval of increased precipitation in the African tropics that persisted until ~5 ka (Gasse, 2000; deMenocal et al., 2000; Garcin et al., 2007). The ages of Rwenzori moraines in the Bujuku and Nyamugasani valleys (~11.7–11 ka) are coincident with this increase in precipitation at the onset of the AHP. However, glacial recession continued after ~11.7 ka and the apparent rapid retreat of Rwenzori glaciers after ~11.2 ka occurred during sustained wet conditions.

Overall, the existing data suggest that Rwenzori glaciers

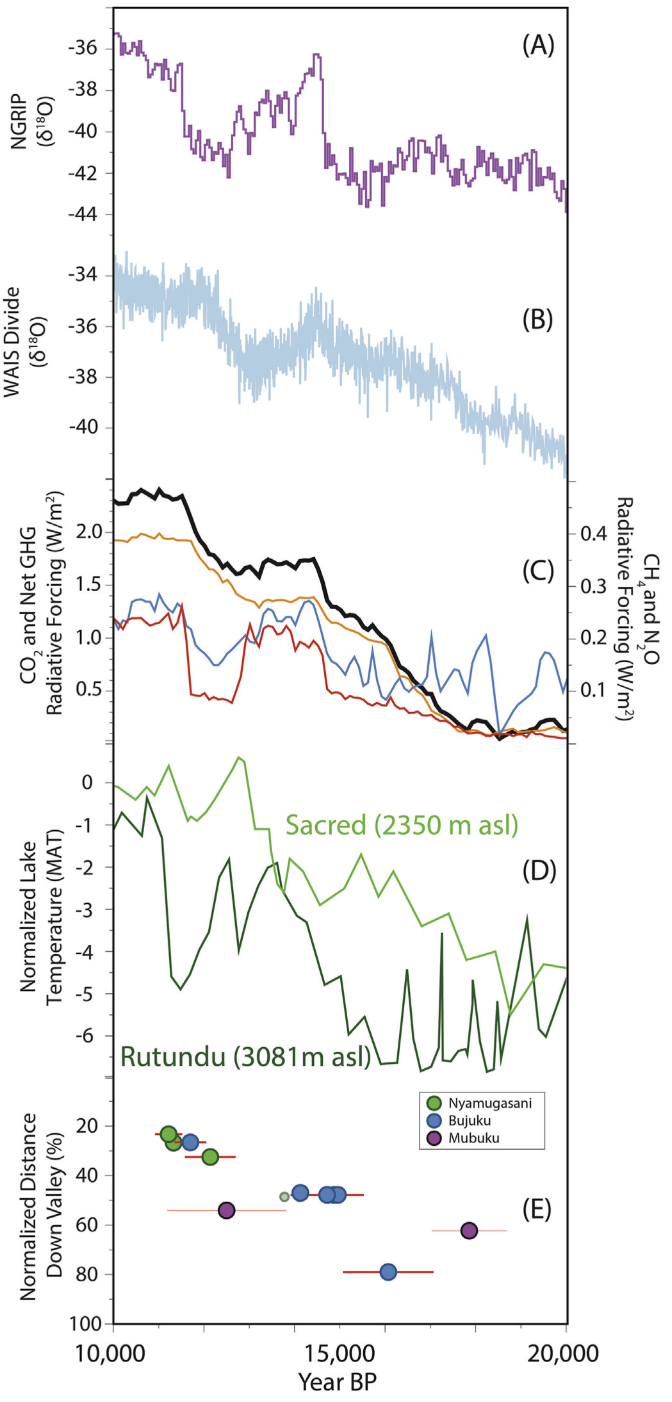

Fig. 8. Temperature and greenhouse gas (GHG) forcing changes during the last deglaciation compared with the Rwenzori glacial chronology. High-latitude temperature records derived from ice cores in (A) Greenland (NGRIP Members, 2004) and (B) Antarctica (WAIS Divide Project Members, 2013) suggest at times antiphased temperature change between the northern and southern hemispheres. (C) Net GHG forcing (black) derived from the summed forcing of CO_2 (orange), CH_4 (red), and N_2O (blue)(Marcott et al., 2014; Rhodes et al., 2015; Ahn and Brook, 2008) and (D) high-elevation temperature reconstructions from alpine lakes on Mt. Kenya (Rutundu, dark green; Sacred, light green) show some similarity, but the inflection points in each record do not align (Loomis et al., 2012, 2017). (E) The Rwenzori glacial chronology, here plotted with mean moraine ages versus the normalized distance downvalley as in Fig. 7, indicates recession during HS1 with slower net recession during the period between ~15 and 11 ka.

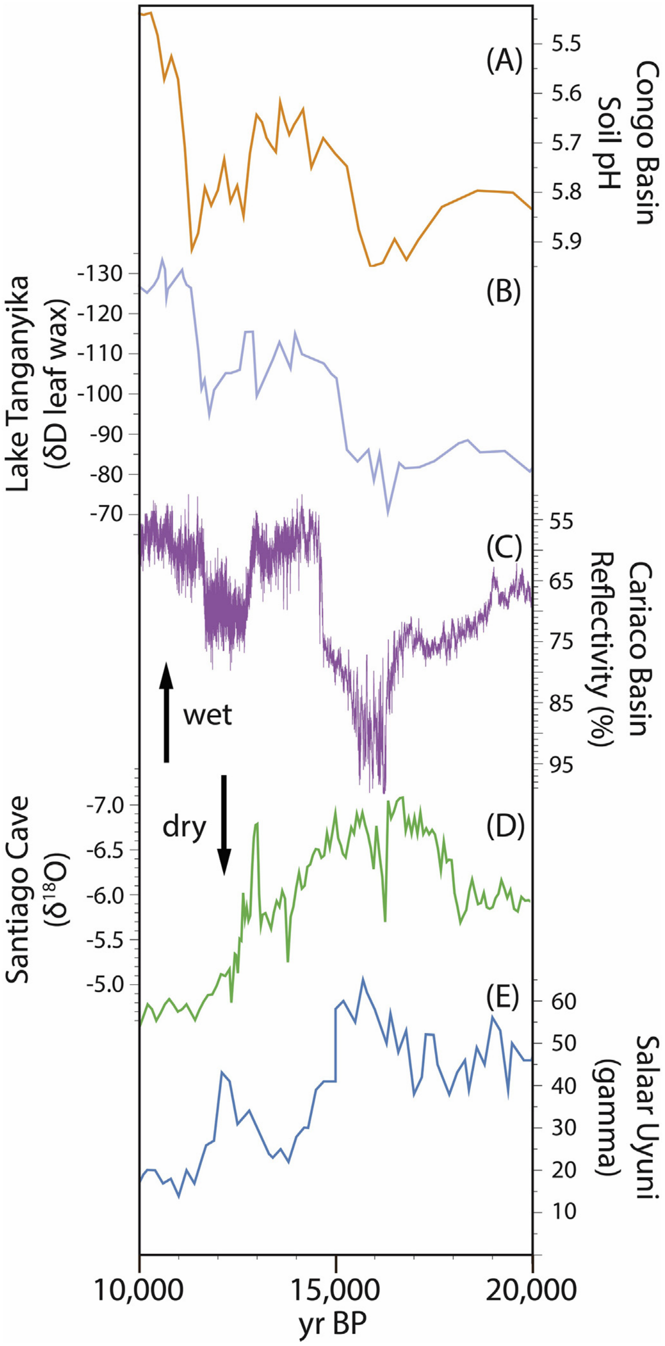

Fig. 9. Precipitation changes in the African and South American tropics during the last glacial termination. Records of relative precipitation change from (A) the Congo Basin (Weijers et al., 2007) and (B) Lake Tanganyika (Tierney et al., 2008) indicate regionally coherent changes in hydroclimate and are similar to precipitation patterns inferred from northern tropical South America such as in (C) the Cariaco Basin (Deplazes et al., 2013). Records of precipitation from (D) Santiago Cave in Ecuador (Mosblech et al., 2012) and from (E) Salaar Uyuni, Bolivia (Baker et al., 2001), suggest precipitation changes different from that in Africa and the northern tropical Andes.

retreated during periods of both elevated and reduced precipitation. For instance, regional aridity during HS1 likely encouraged mass loss; the Bujuku 5 and 4 moraines, deposited coincident with the onset of more humid conditions at ~15 ka, could reflect a temporary slowdown or pause in glacial retreat resulting from elevated precipitation. However recession apparently continued or recommenced shortly after this climatic change point in spite of continued elevated precipitation.

Our comparison of glacial extents with regional climate conditions suggests that the Rwenzori glacial chronology reflects primarily changes in temperature, with some glacial fluctuations modulated by precipitation. This is supported by modern observational and modeling studies of tropical glaciers, including glaciers in the Rwenzori (Rupper and Roe, 2008; Sagredo and Lowell, 2012; Sagredo et al., 2014; Doughty et al., in press). Regional temperature reconstructions vary regarding the timing and magnitude of changes during deglaciation, yet clearly document warming during HS1 and between ~14 and 11 ka. Continued glacial recession during this time in spite of elevated precipitation suggests that any mass balance changes induced by changing precipitation were overcome by the influence of rising temperatures. Recent work modeling past Rwenzori glacial extents using the temperature record from Lake Rutundu (3081 m asl) on Mt. Kenya (Loomis et al., 2017) shows glaciers reaching the late-glacial (~15–11 ka) moraines in the Bujuku valley with a cooling of 4 °C and precipitation decrease of 10% (Doughty et al., in press). Not all East African temperature reconstructions show a late-glacial cooling of this magnitude, but this brGDGT record and glacial reconstruction support a 3–4 °C cooling during the late glacial (Doughty et al., in press).

While there are no independent temperature reconstructions (i.e., not based on glacier extents) from tropical South America during the last glacial termination with which tropical South American glacial fluctuations can be compared, there are many precipitation records for this time. In contrast to the relatively unified precipitation regime in tropical Africa, tropical South America experienced more diverse and often hemispherically antiphased precipitation variations during the last glacial termination (e.g., Novello et al., 2017 and references therein)(Fig. 9). Sites in northern tropical South America experienced relative aridity during HS1 and the YD whereas southern tropical regions were relatively wet during these periods. If precipitation were the primary control on tropical glacial mass balance during deglaciation, one would expect glacial fluctuations in the northern and southern tropical Andes to have exhibited distinct patterns of change, potentially anti-phased between regions (e.g., Mark et al., 2017). In contrast, glaciers in both regions exhibit broadly similar histories.

The apparent coherence of glacial fluctuations in tropical Africa and South America during the last glacial termination, particularly during HS1, suggests that glaciers in both regions responded to a common forcing mechanism. Although precipitation likely modulated glacial mass balance changes, we suggest that temperature exerted greater influence on tropical glaciers during the deglacial warming. Changes in modern tropospheric temperature are communicated rapidly across the low latitudes and, as a result, the tropical troposphere is considered thermally homogenous (Pierrehumbert, 1995; Wu et al., 2001). Presuming that this was the case during the last deglaciation, it may serve as an explanatory mechanism for the propagation of a unified temperature signal across the tropics as reflected by tropical glaciers. Additional work is needed, however, to determine the magnitude and timing of temperature changes in the low latitudes during the last glacial termination, as well as the influence of changing climate conditions on individual glacial catchments.

5.4. Controls on tropical temperature during the last glacial termination

Based on our assessment of tropical glacial chronologies and paleoclimate reconstructions, we suggest that temperature was a dominant influence on glacial fluctuations in the humid inner tropics during the last glacial termination. The driver(s) of tropical temperatures during this period, however, is unclear. Mean-annual equatorial insolation decreased throughout deglaciation (Berger and Loutre, 1991), which would have encouraged tropical glacial advances rather than retreats (Kaser and Osmaston, 2002). Boreal summer insolation rose between ~24 and 11 ka, but whether and how temperature changes in the northern high latitudes driven by this forcing would be transmitted to the tropics is uncertain. Rising boreal summer insolation and increasing austral summer duration may have influenced the onset of tropical deglaciation at ~20–19 ka through a reduction in net heat export from the low latitudes (Jackson et al., 2019); although boreal summer insolation intensity and austral summer duration continued to rise throughout the termination, the large-scale ocean-atmosphere reorganizations that marked the HS1, B-A, ACR, and YD would likely have had a greater influence on tropical climate and heat transport than did far-field insolation effects. In addition, the changes in the rate of ice recession during the last deglaciation inferred across the tropics cannot be explained solely by insolation forcing.

Atmospheric greenhouse gases (GHGs), particularly CO_2, are a primary control on tropical temperatures over glacial-interglacial cycles (Lea, 2004) and may have driven millennial-scale temperature fluctuations (Shakun et al., 2012). Pan-tropical sea-surface temperature reconstructions indicate that deglacial temperature changes were broadly similar to changes in GHG concentrations following the LGM (Shakun et al., 2012). However, tropical glaciers receded from their LGM maximum extents by ~20-19 ka, before the onset of deglacial CO_2 rise at ~18.2 ka (Shakun et al., 2015; Bromley et al., 2016; Jackson et al., 2019). This suggests that low-latitude temperatures were not necessarily coupled with GHG levels at the onset of deglaciation (Shakun et al., 2015; Jackson et al., 2019). Rising atmospheric CO_2 and methane after ~18.2 ka increased net GHG radiative forcing (Marcott et al., 2014), coincident with tropical glacial recession during HS1. Net GHG forcing stagnated during the B-A/ACR and increased at the onset of the YD (Fig. 8); GHG forcing may explain the observed pattern of glacial fluctuations, at least in part. However, many tropical glacial chronologies show an interval of deglacial cooling culminating at ~14 ka, prior to the end of the B-A/ACR (*sensu-stricto* at ~13 ka) and the associated onset of atmospheric CO_2 rise (Lemieux-Dudon et al., 2010). Net GHG forcing again plateaued after ~11.7 ka, as tropical glaciers began to again retreat more rapidly. Although more work is needed to determine the millennial-scale fluctuations of tropical glaciers at all sites, we suggest that GHG forcing alone cannot explain the inferred pattern of tropical glacial fluctuations during the last glacial termination.

The Rwenzori and wider pan-tropical glacial chronologies discussed here show that any explanation for deglacial temperature changes must account for tropical warming during HS1 and likely cooler temperatures during the early B-A/ACR than during the YD. In addition, the manifestations of these abrupt climate events in the high-elevation tropics as inferred from the glacial-geomorphic record do not correlate directly with higher latitude climate changes. Therefore, the terrestrial tropical regions did not adhere to a strictly 'northern' or 'southern' climate pattern. This highlights the tropics as a distinct region for consideration when assessing past temperature changes.

6. Conclusions

Following the onset of deglaciation from the LGM maximum glacial extents, glaciers in the Rwenzori Mountains retreated during HS1 before pausing ~15 ka. Recession continued after ~15–14 ka, though at a slower (net) rate relative to HS1 retreat. Further glacial recession with intermittent moraine deposition after ~11.7 ka was followed by more rapid ice retreat during the early Holocene. The Rwenzori glacial chronology shows fluctuations broadly consistent with glacial fluctuations elsewhere in tropical Africa as well as with similar (i.e., ^{10}Be) glacial chronologies in South America. The apparent coherence of glacial fluctuations in this pan-tropical region suggests that temperature, modulated by regional variations in precipitation, was a dominant influence on glacial extents during the last glacial termination, although more work is needed to assess the millennial-scale pattern of deglaciation at all sites. While the ultimate controls on tropical temperatures during the last deglaciation remain unresolved, the glacial chronology presented here provides important information on the global footprint and expression of deglacial warming and abrupt climate events. Future efforts to date glacial fluctuations in the Rwenzori and elsewhere in the tropics will help elucidate the timing and magnitude of millennial-scale temperature changes. These data are crucial for establishing the drivers of tropical climate change and the role of the tropics in the larger climate system.

Author statement

M.S.J., M.A.K., J.M.R., A.M.D., D.A.C., and M.B.B. conducted fieldwork and collected samples. M.S.J., J.A.H., D.A.C., and M.B.B. processed samples and analyzed results. S.R.H.Z. measured beryllium ratios. M.S.J., M.A.K., J.R.M., and A.M.D. analyzed and interpreted results. B.N. coordinated the project in Uganda. M.S.J. and J.C. made glacial-geomorphic maps. M.S.J. wrote the paper with contributions from all authors. All authors have approved the submitted version of the manuscript.

Declaration of Competing Interest

The authors declare that they have no known competing financial interests or personal relationships that could have appeared to influence the work reported in this paper.

Acknowledgements

We thank the Uganda National Council on Science and Technology and the Uganda Wildlife Authority for their support of and assistance with this project. We also thank Rwenzori Trekking Services and Rwenzori Mountaineering Services for their safety and logistical support while in the field. S. Loomis assisted in sample collection. This project was supported by grants from the National Science Foundation (EAR-1702293; GSS-1558358), National Geographic Society, the Comer Family Foundation, and Sigma Xi. Satellite imagery was granted by the DigitalGlobe Foundation. This is LLNL-JRNL-792707.

References

Ahn, J., Brook, E.J., 2008. Atmospheric CO2 and climate on millennial time scales during the last glacial period. Science 322, 83–85.

Baker, P.A., Rigsby, C.A., Seltzer, G.O., Fritz, S.C., Lowenstein, T.K., Bacher, N.P., Veliz, C., 2001. Tropical climate changes at millennial and orbital timescales on the Bolivian Altiplano. Nature 409, 698–701.

Balco, G., Stone, J.O., Lifton, N.A., Dunai, T.J., 2008. A complete and easily accessible means of calculating surface exposure ages or erosion rates from 10Be and 26Al measurements. Quat. Geochronol. 3, 174–195.

Barker, S., Diz, P., Vautravers, M.J., Pike, J., Knorr, G., Hall, I.R., Broecker, W.S., 2009. Interhemispheric Atlantic seesaw response during the last deglaciation. Nature 457, 1097–1102.

Berger, A., Loutre, M.F., 1991. Insolation values for the last 10 million years. Quat. Sci. Rev. 10, 297–317.

Berke, M.A., Johnson, T.C., Werne, J.P., Livingstone, D.A., Grice, K., Schouten, S., Damste, J.S.S., 2014. Characterization of the last deglacial transition in tropical East Africa: insights from Lake Albert. Palaeogeogr. Palaeoclimatol. Palaeoecol. 409, 1–8.

Beuning, K.R., Talbot, M.R., Kelts, K., 1997. A revised 30,000-year paleoclimatic and paleohydrologic history of Lake Albert, East Africa. Palaeogeogr. Palaeoclimatol. Palaeoecol. 136, 259–279.

Blard, P.H., Braucher, R., Lavé, J., Bourles, D., 2013. Cosmogenic 10Be production rate calibrated against 3He in the high tropical Andes (3800-4900 m, 20-22°S). Earth Planet Sci. Lett. 382, 140–149.

Blunier, T., Brook, E.J., 2001. Timing of millennial-scale climate change in Antarctica and Greenland during the last glacial period. Science 291, 109–112.

Broecker, W.S., Denton, G.H., Edwards, R.L., Cheng, H., Alley, R.B., Putnam, A.E., 2010. Putting the Younger Dryas cold event into context. Quat. Sci. Rev. 29, 1078–1081.

Bromley, G.R.M., Schaefer, J.M., Hall, B.L., Rademaker, K.M., Putnam, A.E., Todd, C.E., Hegland, M., Winckler, G., Jackson, M.S., Strand, P.D., 2016. A cosmogenic 10Be chronology for the local last glacial maximum and termination in the Cordillera Oriental, southern Peruvian Andes: implications for the tropical role in global climate. Quat. Sci. Rev. 148, 54–67.

deMenocal, P., Ortiz, J., Guilderson, T., Adkins, J., Sarnthein, M., Baker, L., Yarusinsky, M., 2000. Abrupt onset and termination of the African Humid Period: rapid climate responses to gradual insolation forcing. Quat. Sci. Rev. 19, 347–361.

Denton, G.H., Anderson, R.F., Toggweiler, J.R., Edwards, R.L., Schaefer, J.M., Putnam, A.E., 2010. The last glacial termination. Science 328, 1652–1656.

Deplazes, G., Lückge, A., Peterson, L.C., Timmermann, A., Hamann, Y., Hughen, K.A., Röhl, U., Laj, C., Cane, M.A., Sigman, D.M., Haug, G.H., 2013. Links between tropical rainfall and North Atlantic climate during the last glacial period. Nat. Geosci. 6, 213–217.

Diaz, H.F., Eischeid, J.K., Duncan, C., Bradley, R.S., 2003. Variability of freezing levels, melting season indicators, and snow cover for selected high-elevation and continental regions in the last 50 years. Climate Variability and Change in High Elevation Regions: Past, Present & Future. Springer, Dordrecht, pp. 33–52.

Doughty, A.M., Kelly, M.A., Russell, J.M., Jackson, M.S., Anderson, B.M., Chipman, J., Nakileza, B., and Dee, S.G. The dynamics of equilibrium line altitudes in over the past 31,000 years in the Rwenzori Mountains, East Africa. GSA Special Paper on Quaternary Science in Honor of Prof. Stephen C. Porter [(in press)].

Dunai, T.J., 2010. Cosmogenic Nuclides: Principles, Concepts and Applications in the Earth Surface Sciences. Cambridge University Press.

Foster, P., 2001. The potential negative impacts of global climate change on tropical montane cloud forests. Earth Sci. Rev. 55, 73–106.

Garcin, Y., Vincens, A., Williamson, D., Buchet, G., Guiot, J., 2007. Abrupt resumption of the african monsoon at the Younger Dryas—Holocene climatic transition. Quat. Sci. Rev. 26, 690–704.

Gasse, F., 2000. Hydrological changes in the African tropics since the Last Glacial Maximum. Quat. Sci. Rev. 19, 189–211.

Hamilton, A.C., 1982. Environmental History of East Africa: a Study of the Quaternary. Academic press, London, p. 328.

Hamilton, A., Perrott, A., 1978. Date of deglacierisation of Mount Elgon. Nature 273, 49.

Jackson, M.S., Kelly, M.A., Russell, J.M., Doughty, A.M., Howley, J.A., Chipman, J.W., Cavagnaro, D.B., Zimmerman, S.R.H., Nakileza, B., 2019. High-latitude warming initiated the onset of the last deglaciation in the tropics. Science Advances 5, eaaw2610.

Jomelli, V., Favier, V., Vuille, M., Braucher, R., Martin, L., Blard, P.H., Colose, C., Brunstein, D., He, F., Khodri, M., Bourlès, D.L., Leanni, L., Rinterknecht, V., Grancher, D., Francou, B., Ceballos, J.L., Fonseca, H., Liu, Z., Otto-Bliesner, B.L., 2014. A major advance of tropical Andean glaciers during the Antarctic cold reversal. Nature 513, 224–228.

Jomelli, V., Martin, L., Blard, P.H., Favier, V., Vuille, M., Ceballos, J.L., 2017. Revisiting the Andean tropical glacier behavior during the Antarctic cold reversal. Cuadernos de Investigación Geográfica 43, 629–20.

Kaser, G., Osmaston, H., 2002. Tropical Glaciers. Cambridge University Press.

Kelly, M.A., 2003. The Late Würmian Age in the Western Swiss Alps: Last Glacial Maximum (LGM) Ice-Surface Reconstruction and 10Be Dating of Late-Glacial Features. Doctoral dissertation. Verlag nicht ermittelbar.

Kelly, M.A., Russell, J.M., Baber, M.B., Howley, J.A., Loomis, S.E., Zimmerman, S., Nakileza, B., Lukaye, J., 2014. Expanded glaciers during a dry and cold last glacial maximum in equatorial East Africa. Geology 42, 519–522.

Kelly, M.A., Lowell, T.V., Applegate, P.J., Phillips, F.M., Schaefer, J.M., Smith, C.A., Kim, H., Leonard, K.C., Hudson, A.M., 2015. A locally calibrated, late glacial 10Be production rate from a low-latitude, high-altitude site in the Peruvian Andes. Quat. Geochronol. 26, 70–85.

Lal, D., 1991. Cosmic ray labeling of erosion surfaces: in situ nuclide production rates and erosion models. Earth Planet Sci. Lett. 104, 424–439.

Lea, D.W., 2004. The 100 000-yr cycle in tropical SST, greenhouse forcing, and climate sensitivity. J. Clim. 17, 2170–2179.

Lemieux-Dudon, B., Blayo, E., Petit, J.R., Waelbroeck, C., Svensson, A., Ritz, C., Barnola, J.M., Narcisi, B.M., Parrenin, F., 2010. Consistent dating for Antarctic and Greenland ice cores. Quat. Sci. Rev. 29, 8–20.

Lentini, G., Cristofanelli, P., Duchi, R., Marinoni, A., Verza, G., Vuillermoz, E., Toffolon, R., Bonasoni, P., 2011. Mount Rwenzori (4750 M asl, Uganda): meteorological characterization and air-mass transport analysis. Geogr. Fis. Din. Quaternaria 34, 183–193.

Lifton, N., Sato, T., Dunai, T.J., 2014. Scaling in situ cosmogenic nuclide production rates using analytical approximations to atmospheric cosmic-ray fluxes. Earth Planet Sci. Lett. 386, 149–160.

Livingstone, D.A., 1962. Age of deglaciation in the Ruwenzori range, Uganda. Nature 194, 859–860.

Livingstone, D.A., 1967. Postglacial vegetation of the Ruwenzori Mountains in equatorial Africa. Ecol. Monogr. 37, 25–52.

Loomis, S.E., Russell, J.M., Ladd, B., Street-Perrott, F.A., Damsté, J.S.S., 2012. Calibration and application of the branched GDGT temperature proxy on East African lake sediments. Earth Planet Sci. Lett. 357–358, 277–288.

Loomis, S.E., Russell, J.M., Verschuren, D., Morrill, C., De Cort, G., Damsté, J.S.S., Olago, D., Eggermont, H., Street-Perrott, F.A., Kelly, M.A., 2017. The tropical lapse rate steepened during the Last Glacial Maximum. Science Advances 3, e1600815.

Mahaney, W.C., 1982. Chronology of glacial and periglacial deposits, Mount Kenya, East Africa: descriptions of type sections. Paleoecology of Africa 14, 25–43.

Marcott, S.A., Bauska, T.K., Buizert, C., Steig, E.J., Rosen, J.L., Cuffey, K.M., Fudge, T.J., Severinghaus, J.P., Ahn, J., Kalk, M.L., McConnell, J.R., Sowers, T., Taylor, K.C., White, J.W.C., Brook, E.J., 2014. Centennial-scale changes in the global carbon cycle during the last deglaciation. Nature 514, 616–619.

Mark, B., Stansell, N., Zeballos, G., 2017. The last deglaciation of Peru and Bolivia. Cuadernos de Investigación Geográfica 43, 591–32.

McConnell, R.B., 1959. Outline of the Geology of the Ruwenzori Mountains: A Preliminary Account of the Results of the British Ruwenzori Expedition, 1951-1952. HM Stationery Office.

Mölg, T., Georges, C., Kaser, G., 2003a. The contribution of increased incoming shortwave radiation to the retreat of the Rwenzori glaciers, East Africa, during the 20th century. Int. J. Climatol. 23, 291–303.

Mölg, T., Hardy, D.R., Kaser, G., 2003b. Solar-radiation-maintained glacier recession on Kilimanjaro drawn from combined ice-radiation geometry modeling. J. Geophys. Res.: Atmosphere 108 (D23).

Mosblech, N.A., Bush, M.B., Gosling, W.D., Hodell, D., Thomas, L., Van Calsteren, P., Correa-Metrio, A., Valencia, B.G., Curtis, J., Van Woesik, R., 2012. North Atlantic forcing of Amazonian precipitation during the last ice age. Nat. Geosci. 5, 817–820.

NGRIP Members, 2004. High-resolution record of Northern Hemisphere climate extending into the last interglacial period. Nature 431, 147–151.

Nishiizumi, K., Imamura, M., Caffee, M.W., Southon, J.R., Finkel, R.C., McAninch, J., 2007. Absolute calibration of 10Be AMS standards. Nucl. Instrum. Methods Phys. Res. Sect. B Beam Interact. Mater. Atoms 258, 403–413.

Novello, V.F., Cruz, F.W., Vuille, M., Stríkis, N.M., Edwards, R.L., Cheng, H., Emerick, S., de Paula, M.S., Li, X., de S Barreto, E., Karmann, I., Santos, R.V., 2017. A high-resolution history of the south American monsoon from last glacial maximum to the Holocene. Sci. Rep. 7, 44267.

Osmaston, H.A., 1965. The Past and Present Climate and Vegetation of Ruwenzori and its Neighbourhood. Doctoral dissertation. University of Oxford.

Osmaston, H., 1989. Glaciers, glaciations and equilibrium line altitudes on the Rwenzori. In: Mahaney, W.C. (Ed.), Quaternary and Environmental Research on East African Mountains. Balkema, Rotterdam, pp. 31–104.

Osmaston, H., 2006. Guide to the Rwenzori: the Mountains of the Moon. Rwenzori Trust, p. 336.

Ossendörf, G., Groos, A.R., Bromm, T., Tekelemariam, M.G., Glaser, B., Lesur, J., Schmidt, J., Akçar, N., Bekele, T., Beldados, A., Demissew, S., Kahsay, T.H., Nash, B.P., Nauss, T., Negash, A., Nemomissa, S., Veit, H., Vogelsang, R., Woldu, Z., Zech, W., Opgenoorth, L., Miehe, G., 2019. Middle Stone Age foragers resided in high elevations of the glaciated Bale Mountains, Ethiopia. Science 365, 583–587.

Otto-Bliesner, B.L., Russell, J.M., Clark, P.U., Liu, Z., Overpeck, J.T., Konecky, B., deMenocal, P., Nicholson, S.E., He, F., Lu, Z., 2014. Coherent changes of southeastern equatorial and northern African rainfall during the last deglaciation. Science 346, 1223–1227.

Pentecost, A., 1998. Some observations on the biomass and distribution of cryptogamic epiphytes in the upper montane forest of the Rwenzori Mountains, Uganda. Global Ecol. Biogeogr. 7, 273–284.

Pierrehumbert, R.T., 1995. Thermostats, radiator fins, and the local runaway greenhouse. J. Atmos. Sci. 52, 1784–1806.

Pierrehumbert, R.T., 2000. Climate change and the tropical Pacific: the sleeping dragon wakes. Proc. Natl. Acad. Sci. Unit. States Am. 97, 1355–1358.

Plug, L.J., Gosse, J.C., McIntosh, J.J., Bigley, R., 2007. Attenuation of cosmic ray flux in temperate forest. J. Geophys. Res.: Earth Surface 112, F02022.

Powers, L.A., Johnson, T.C., Werne, J.P., Castañeda, I.S., Hopmans, E.C., Damsté, J.S.S., Schouten, S., 2005. Large temperature variability in the southern african tropics since the last glacial maximum. Geophys. Res. Lett. 32, L08706.

Rasmussen, S.O., Andersen, K.K., Svensson, A.M., Steffensen, J.P., Vinther, B.M., Clausen, H.B., Siggaard-Andersen, M.L., Johnsen, S.J., Larsen, L.B., Dahl-Jensen, D., Bigler, M., Röthlisberger, R., Fischer, H., Goto-Azuma, K., Hansson, M.E., Ruth, U., 2006. A new Greenland ice core chronology for the last glacial termination. J. Geophys. Res. 111, 527–15.

Reimer, P.J., Bard, E., Bayliss, A., Beck, J.W., Blackwell, P.G., Ramsey, C.B., Buck, C.E., Cheng, H., Edwards, R.L., Friedrich, M., Grootes, P.M., 2013. IntCal13 and Marine13 radiocarbon age calibration curves 0–50,000 years cal BP. Radiocarbon 55, 1869–1887.

Rhodes, R.H., Brook, E.J., Chiang, J.C.H., Blunier, T., Maselli, O.J., McConnell, J.R., Romanini, D., Severinghaus, J.P., 2015. Enhanced tropical methane production in response to iceberg discharge in the North Atlantic. Science 348, 1015–1019.

Rupper, S., Roe, G., 2008. Glacier changes and regional climate: a mass and energy balance approach. J. Clim. 21, 5384–5401.

Sagredo, E.A., Lowell, T.V., 2012. Climatology of Andean glaciers: a framework to understand glacier response to climate change. Global Planet. Change 86–87, 101–109.

Sagredo, E.A., Rupper, S., Lowell, T.V., 2014. Sensitivities of the equilibrium line altitude to temperature and precipitation changes along the Andes. Quat. Res. 81, 355–366.

Schaefer, J.M., Denton, G.H., Kaplan, M., Putnam, A., Finkel, R.C., Barrell, D.J., Andersen, B.G., Schwartz, R., Mackintosh, A., Chinn, T., Schlüchter, C., 2009. High-frequency Holocene glacier fluctuations in New Zealand differ from the northern signature. Science 324, 622–625.

Shakun, J.D., Clark, P.U., He, F., Marcott, S.A., Mix, A.C., Liu, Z., Otto-Bliesner, B., Schmittner, A., Bard, E., 2012. Global warming preceded by increasing carbon dioxide concentrations during the last deglaciation. Nature 484, 49–54.

Shakun, J.D., Clark, P.U., Marcott, S.A., Brook, E.J., Lifton, N.A., Caffee, M., Shakun, W.R., 2015. Cosmogenic dating of Late Pleistocene glaciation, southern tropical Andes, Peru. J. Quat. Sci. 30, 841–847.

Shanahan, T.M., Zreda, M., 2000. Chronology of Quaternary glaciations in east Africa. Earth Planet Sci. Lett. 177, 23–42.

Singarayer, J.S., Burrough, S.L., 2015. Interhemispheric dynamics of the African rainbelt during the late Quaternary. Quat. Sci. Rev. 124, 48–67.

Sobel, A.H., Bretherton, C.S., 2000. Modeling tropical precipitation in a single column. J. Clim. 13, 4378–4392.

Stansell, N.D., Licciardi, J.M., Rodbell, D.T., Mark, B.G., 2017. Tropical ocean-atmospheric forcing of late glacial and Holocene glacier fluctuations in the cordillera blanca, Peru. Geophys. Res. Lett. 44, 4176–4185.

Stone, J.O., 2000. Air pressure and cosmogenic isotope production. J. Geophys. Res.: Solid Earth 105, 23753–23759.

Stuiver, M., Reimer, P.J., Reimer, R.W., 2019. CALIB 7.1 at. http://calib.org.

Taylor, R.G., Mileham, L., Tindimugaya, C., Majugu, A., Muwanga, A., Nakileza, B., 2006. Recent glacial recession in the Rwenzori Mountains of East Africa due to rising air temperature. Geophys. Res. Lett. 33, L10402.

Tiercelin, J.J., Gibert, E., Umer, M., Bonnefille, R., Disnar, J.R., Lézine, A.-M., Hureau-Mazaudier, D., Travi, Y., Keravis, D., Lamb, H.F., 2008. High-resolution sedimentary record of the last deglaciation from a high-altitude lake in Ethiopia. Quat. Sci. Rev. 27, 449–467.

Tierney, J.E., Russell, J.M., Huang, Y., Damsté, J., 2008. Northern hemisphere controls on tropical southeast African climate during the past 60,000 years. Science 322, 252–255.

WAIS Divide Project Members, 2013. Onset of deglacial warming in West Antarctica driven by local orbital forcing. Nature 500, 440–444.

Weijers, J.W.H., Schefuss, E., Schouten, S., Damste, J.S.S., 2007. Coupled thermal and hydrological evolution of tropical Africa over the last deglaciation. Science 315, 1701–1704.

Wu, Z., Sarachik, E.S., Battisti, D.S., 2001. Thermally driven tropical circulations under Rayleigh friction and Newtonian cooling: analytic solutions. J. Atmos. Sci. 58, 724–741.